Chair of Hydrology

Albert-Ludwigs-University Freiburg i. Br.

Andrea Popp

Characterization of Spatial and Temporal Artificial Recharge: Field Testing and Numerical Modeling

Master's Thesis

Examiner: Prof. Dr. Markus Weiler (University of Freiburg)

Second examiner: Prof. Dr. Mario Schirmer (Eawag/University of Neuchâtel)

Freiburg i. Br., June 2015

Table of Contents

Acknowledgments

I would like to thank Prof. Dr. Weiler and Prof. Dr. Schirmer for supervising this thesis.

I am especially thankful to Prof. Dr. Schirmer for conferring me the opportunity to pursue my interests in hydrogeological research with his team at Eawag, the Swiss Federal Institute of Aquatic Science and Technology in Dübendorf (Switzerland). I am particularly grateful for his mentoring and the many possibilities he opened up for me.

Additionally, I would like to express my gratitude to Dr. Christian Möck for his patience and outstanding support during this thesis.

List of Figures

List of Tables

Abstract

Water resources management in urban areas is challenging due to different kinds of water usage and water contamination. It is particularly difficult to locate the source of contamination when former landfills and industrial sites are present. The chosen site is located in the canton Basel-Landschaft in Switzerland where drinking water is obtained by artificial groundwater recharge. Water from the river Rhine is withdrawn and put on an excavated system of channels and ponds. However, the abstracted water for the drinking water production contains low concentrations of contaminants. This study is part of the project "Regionale Wasserversorgung Basel-Landschaft 21", which aims to identify the source of pollution and to develop a groundwater management tool to minimize the risk potential for contamination. A key factor to efficiently manage the water abstraction site is the understanding of the artificial groundwater recharge. Hence, the objective of this study is to characterize the spatial and temporal infiltration. A combination of field testing and numerical modeling was applied to investigate the governing processes of the system and to identify the most influencing factors for the infiltration. The results showed that the the infiltration rates are spatially highly heterogeneous, which mainly depends on the distribution of water on the infiltration system. Furthermore, we identified parameters such as the water levels, the clogging layer thickness, the depth to the groundwater table, and the clogging layer and aquifer material to have a strong influence on the infiltration. With the results of this study, we were able to characterize the spatial and temporal infiltration. Subsequently, we can implement systematic actions for an improved management at the water abstraction site.

Key words: artificial groundwater recharge, infiltration, groundwater contamination, numerical modeling, groundwater management

Kurzfassung

In urbanen Gebieten ist Wasserressourcen-Management eine Herausforderung auf Grund verschiedenster Arten von Wassernutzung und Wasserkontamination. Dabei ist es besonders schwierig, die Quelle der Kontamination ausfindig zu machen, wenn Altdeponien und Industrieanlagen vorhanden sind. Das Studiengebiet befindet sich im Kanton Basel-Landschaft in der Schweiz, wo Trinkwasser durch künstliche Grundwasseranreicherung gewonnen wird. Dafür wird Wasser aus dem Rhein entnommen und in ein künstlich geschaffenes System von Kanälen und Weihern gepumpt. Das dem Gebiet entnommene Wasser enthält jedoch in geringen Konzentrationen Spurenstoffe an Kontaminationen. Die hier vorgestellte Studie ist Teil des Projekts „Regionale Wasserversorgung Basel-Landschaft 21“, das beabsichtigt, die Quelle der Kontamination zu identifizieren und einen Grundwassermanagement-Plan zu erstellen, um das Gefährdungspotential für Kontaminationen zu minimieren. Ein Schlüsselfaktor für ein effizientes Management der Wassergewinnungsanlage ist das Verständnis der künstlichen Grundwasseranreicherung. Daher ist das Ziel dieser Studie, die zeitliche und räumliche Infiltration zu beschreiben. Eine Kombination aus Feldarbeit und numerischer Modellierung wurde angewandt, um die das System steuernden Prozesse zu untersuchen und die wichtigsten Einflussfaktoren auf die Infiltration zu identifizieren. Die Ergebnisse der Studie zeigten, dass die Infiltrationsraten räumlich sehr heterogen sind, was hauptsächlich aus der unterschiedlichen Verteilung des Wassers im Infiltrationssystem resultiert. Außerdem konnten Parameter wie die Wasserstände in den Kanälen, die Mächtigkeit des Flussbettes, der Flurabstand zum Grundwasser und die gesättigten hydraulischen Leitfähigkeiten des Flussbett- und Aquifermaterials als wichtige Einflussfaktoren auf die Infiltration identifiziert werden. Mit den Ergebnissen dieser Studie konnten wir die zeitliche und räumliche Infiltration charakterisieren und somit gezielte Maßnahmen zu einem

verbesserten Wassermanagement im Studiengebiet entwickeln.

Schlüsselworte: künstliche Grundwasseranreicherung, Infiltration, Grundwasserkontamination, numerische Modellierung, Grundwasser Management

1

Introduction

As the world population continues to expand, both groundwater and surface water resources are put under stress due to rising water demands. However, groundwater aquifers store more than 98% of the world's liquid freshwater, hence it is a dominant water resource in many parts of the world. Since groundwater is of limited extent, increasing water demands particularly put stress on the drinking water production (Sophocleous, 2002).

To overcome rising water demands artificial groundwater recharge was invented. Artificial groundwater recharge is a technique where in most cases surface water is put on or in the ground to infiltrate and subsequently replenish the underlying aquifer. However, this method does not only aim to meet increasing water demands. Other objectives are (i) to prohibit groundwater depletion, (ii) to store water underground, (iii) to improve the water quality by purification while the water passages the soil, (iv) to use aquifers as conveyance systems, and (v) to create an elevated local groundwater mound preventing water inflow of adjacent areas, which might hold risk potentials. Thus, groundwater is a more reliable source of freshwater compared to surface water. The practice of artificial groundwater recharge becomes increasingly important for a more sustainable water use and is expected to expand in many parts of the world (Bouwer, 2002; Greskowiak et al., 2005; Pedretti et al., 2012; Mair et al., 2013; Bhuiyan, 2015).

2

Background

This master's thesis is integrated into sub-project 3 of the project "Regionale Wasserversorgung Basel-Landschaft 21", a joint cooperation of the "Kompetenzzentrum Trinkwasser" of Eawag and the canton Basel-Landschaft in Switzerland. Its goal is to improve the canton's water use strategy to guarantee the future drinking water supply of about 200 000 people.

2.1 Study Area

In the 1950s, the state-owned waterworks "Hardwasser AG" established groundwater use at the study site to provide drinking water and water for industrial purposes for the canton Basel-Landschaft. The green area in Figure 2.1 represents the study site "Hardwald". It is located in northern Switzerland on the river Rhine and at the border to Germany as indicated in the top right panel of Figure 2.1. The water abstraction area is about 4.65 km^2 large and forested.

Since 1958, natural groundwater has not been sufficient anymore to provide enough water for a growing population and industry. Therefore, the Hardwasser AG started using artificial groundwater recharge as a technique to augment the natural groundwater resources. The recharge is performed by putting surface water originating from the river Rhine on an excavated system of channels and ponds, which is also shown in Figure 2.1. The water naturally infiltrates from the top surface to the underlying aquifer. The rectangular shaped channels are about 2 m wide and reach a total length of approximately 2.3 km. The ponds are more or less circular and

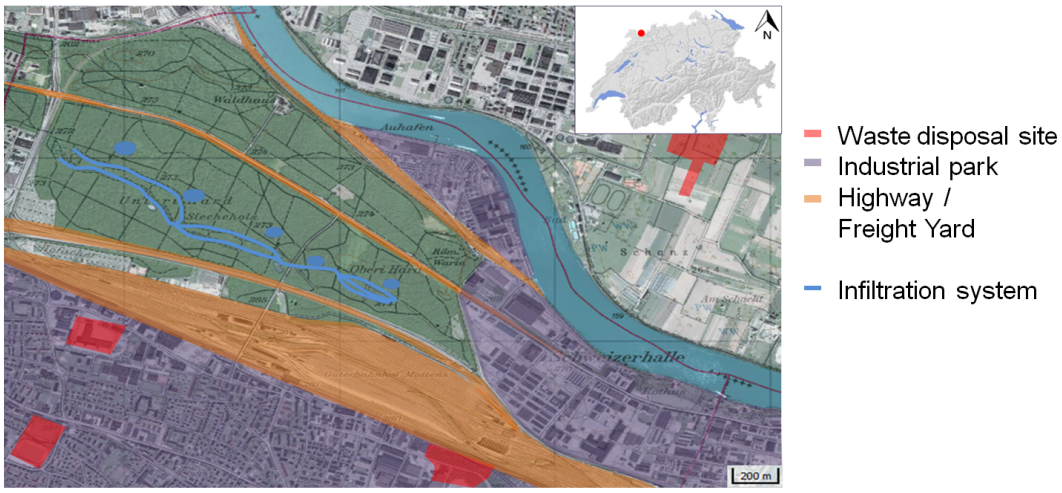

Figure 2.1: Study area "Hardwald" with the infiltration system and potential contamination sites.

occupy a total area of about 10 km^2.

Figure 2.1 also illustrates the exposure of the Hardwald to potential contamination due to surrounding industry, former waste disposal sites, a highway and freight depots. Thus, the artificial groundwater recharge does not only serve the purpose to overcome increasing water demands, but also to protect the area against peripheral influences. This is accomplished by recharging twice as much water as is required and abstracted. As a result of that, an elevated local groundwater mound is created, which functions as a natural barrier preventing the inflow of potentially contaminated water coming from adjacent areas (Meier, 2014). The concept of this method is schematically shown in Figure 2.2. Additionally, the artificial groundwater recharge facilitates the natural filtration of the soil to improve the river water quality and to store water underground to tide over accidental pollution of the river water (Bouwer, 2002).

However, despite the efforts of prohibiting contaminants to enter the system, low concentrations of trace compounds such as hexachlorbutadiene or trichloromethane can be found in the extracted water (Affolter et al., 2010). The hypothesis regarding the origin of the contaminants is that the pollution is a result of remobilisation of contaminants and changing hydraulic conditions, which affect the flow direction of the contaminant plumes (Auckenthaler et al., 2010; Matousek et al., 2011). The contamination is below drinking water limits, but as a precaution it passes an acti-

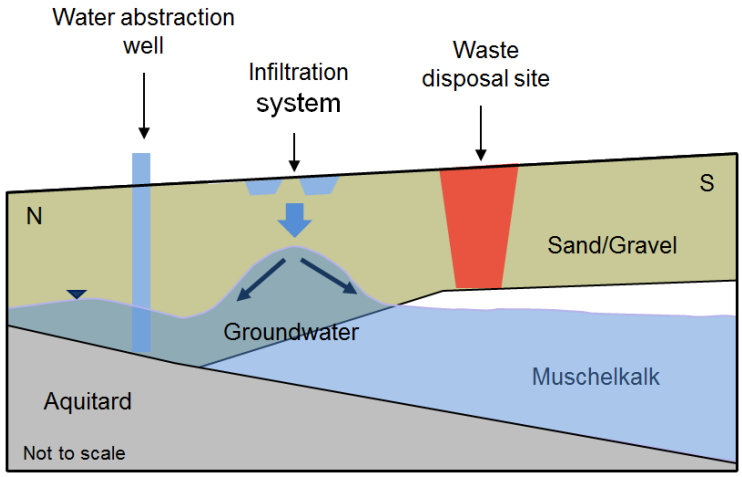

Figure 2.2: Cross-section showing how the elevated groundwater mound is supposed to prohibit contaminated water inflow from contamination sites (here exemplarily a former waste disposal site) to the water abstraction wells.

vated carbon filtration before entering the public water supply. However, an end of pipe solution is not desirable.

2.2 Research Objectives and Outline

The main objective of sub-project 3 is to identify current and future risk potentials by investigating the water quality of observation and pumping wells, and by numerical simulations of flow and transport processes under various operating modes. With the applied methods the study aims to detect the origin of the trace compounds. Finally, an adaptive groundwater management tool will be developed, which enables an operating mode with the lowest risk potential.

With this master's thesis, we aim to characterize the spatial and temporal variability of artificial groundwater recharge. Thorough knowledge of the processes and most influential factors governing the infiltration is crucial for an efficient water management at the presented site.

The combined approach of field testing and numerical modeling we used is shown in Figure 2.3. First, field testings were conducted to measure the groundwater table elevations, several groundwater parameters, and stream water levels. The observations were then used to estimate the spatial and temporal infiltration at the study site. Furthermore, the results from the field measurements served as basis and validation

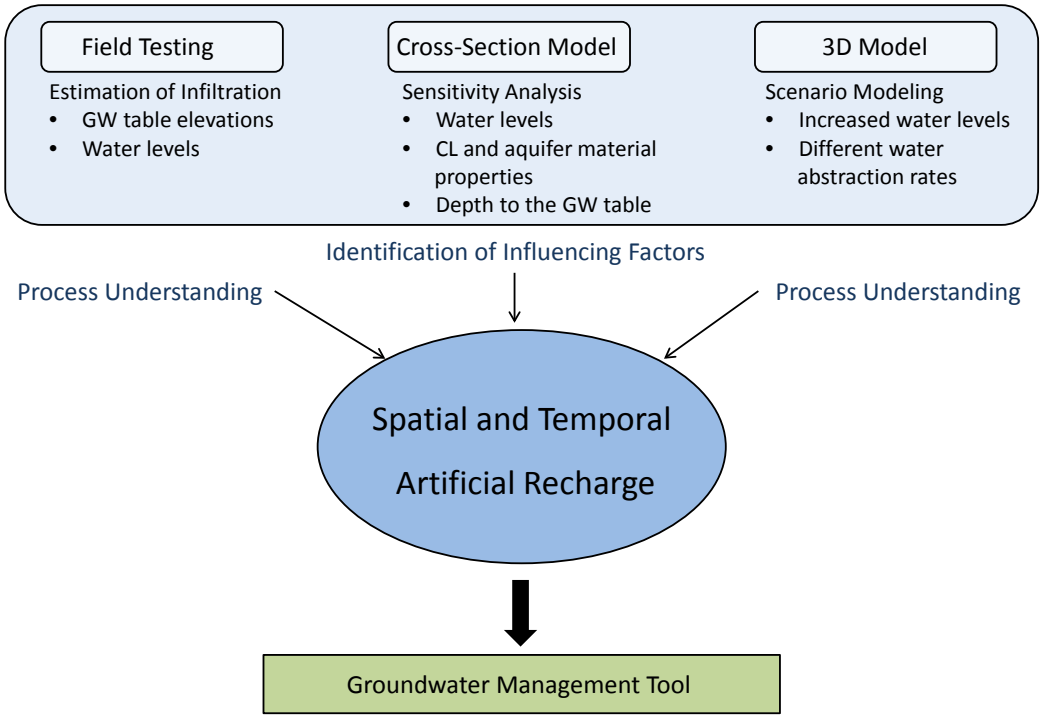

Figure 2.3: Structure of the thesis.

for the following numerical modeling. Subsequently, two numerical models were set up. The first cross-section model was built for sensitivity analyses of a segment of the study site. The model was used to identify the impact of (i) different water levels in the infiltration channels, (ii) the clogging layer (CL) thickness and the depth to the water table, and (iii) the clogging layer and aquifer material properties. Next, a 3D model, which represents the whole study area was build. This model is based on the results of the cross-section model and incorporates the observed groundwater table elevations. The 3D model was used to simulate scenarios for different water injection and abstraction rates with the aim to understand the impact of extreme operating modes on the groundwater table elevations and stream fluxes. Finally, all results will contribute to the development of the groundwater management tool.

3

Field Testing

A combination of different methods was required to characterize the infiltration processes. First, we conducted field tests to determine the temporal and spatial infiltration rates.

3.1 Groundwater Measurements

In two large field campaigns in November 2014 and March 2015, groundwater (GW) table elevations of 44, respectively 37 observation and pumping wells were surveyed. The second field campaign in March was necessary, since the channel water levels in November were below average. Since we wanted to observe the general condition of the system, we conducted a second field campaign in March, when we observed mean water levels. Hence, in this study only the data of the March field campaign were used.

Additionally, we acquired water samples for the analysis of stable water isotopes, (in)organic compounds, and other groundwater parameters such as temperature and conductivity by groundwater pumping. Figure 3.1 illustrates linearly interpolated observations of the groundwater conductivity, which shows increased values in the western part of the study area. This might be connected either to different geology or to increased contaminant concentrations in this area. The latter theory is consistent with measurements of 58 in wells screened contaminants in the March field campaign (partly sampled by an engineering office). Figure 3.2 shows exemplarily the distribution of the contaminant “tetrachloroethene”, also called “perchloroethy-

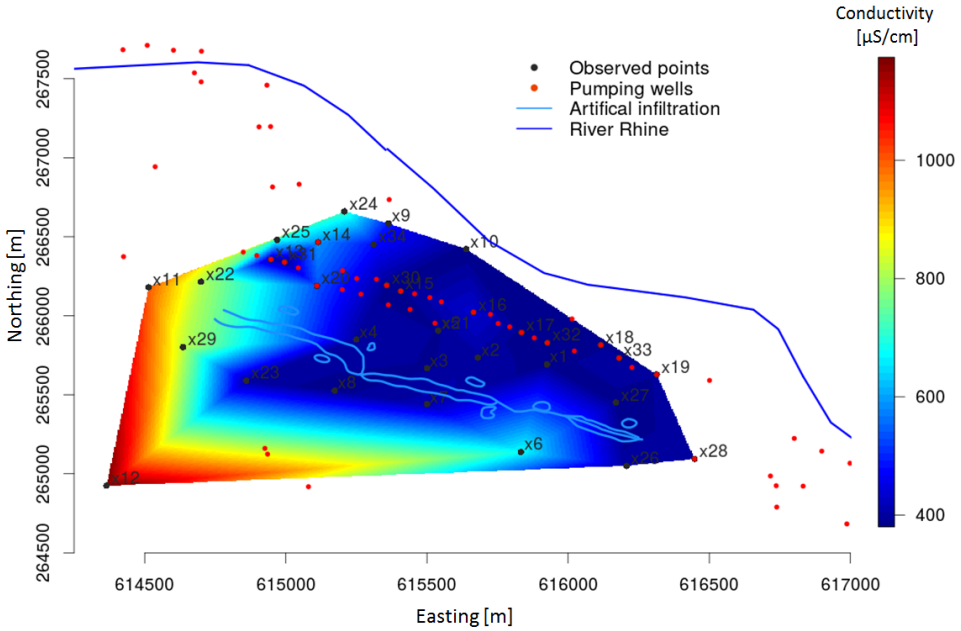

Figure 3.1: Linearly interpolated groundwater conductivity observed at 34 points in March 2015.

lene", on a logarithmic scale. Tetrachloroethene is, among others, used for metal degreasing operations (US Environmental Protection Agency, 2012). The distribution shows the highest concentrations at the western part of the infiltration system.

Figure 3.3 shows linearly interpolated water table elevations of 34 observed wells (3 of the originally 37 observed wells had fallen dry) based on the groundwater table observations of the field campaign in March. As expected, the highest elevations are close to the artificial infiltration system as well as in the south-western part of the study area. The elevations decrease towards the river Rhine.
Later, we implemented these observations in the cross-section model (see Section 5.2) and used them to validate the 3D model (see Section 5.3).

3.2 Discharge and Water Level Measurements

To estimate the infiltration of each channel segment we conducted discharge and water level measurements at the water inflow and outflow of each channel segment (except for channels 7 and 8, where no outflow measurements is needed since all water is being infiltrated by the end of the system; see Figure 3.4). From now

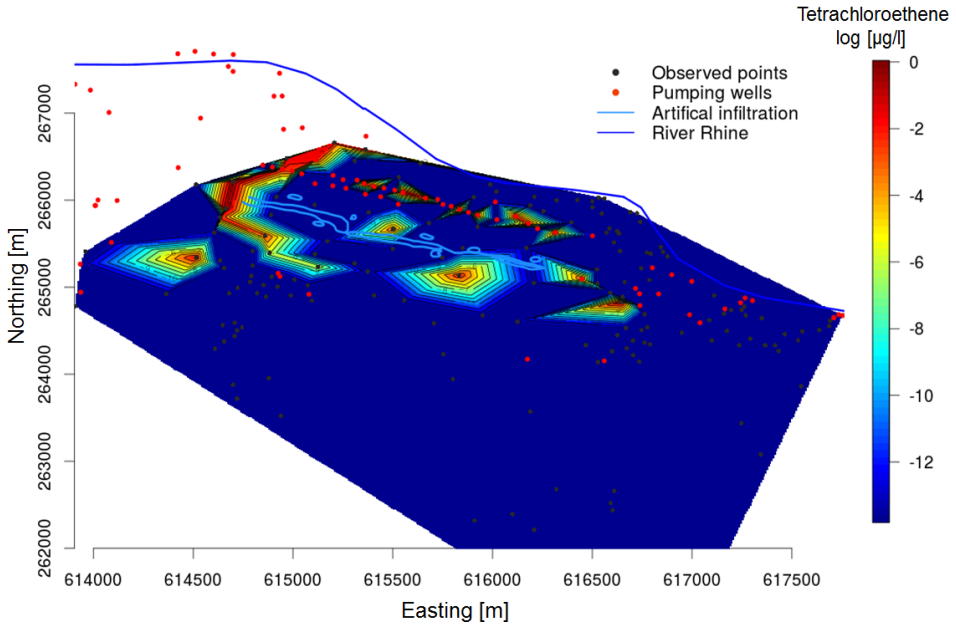

Figure 3.2: Linearly interpolated distribution of the contaminant "tetrachloroethene" (on a logarithmic scale) observed in 58 wells in the study area in March 2015.

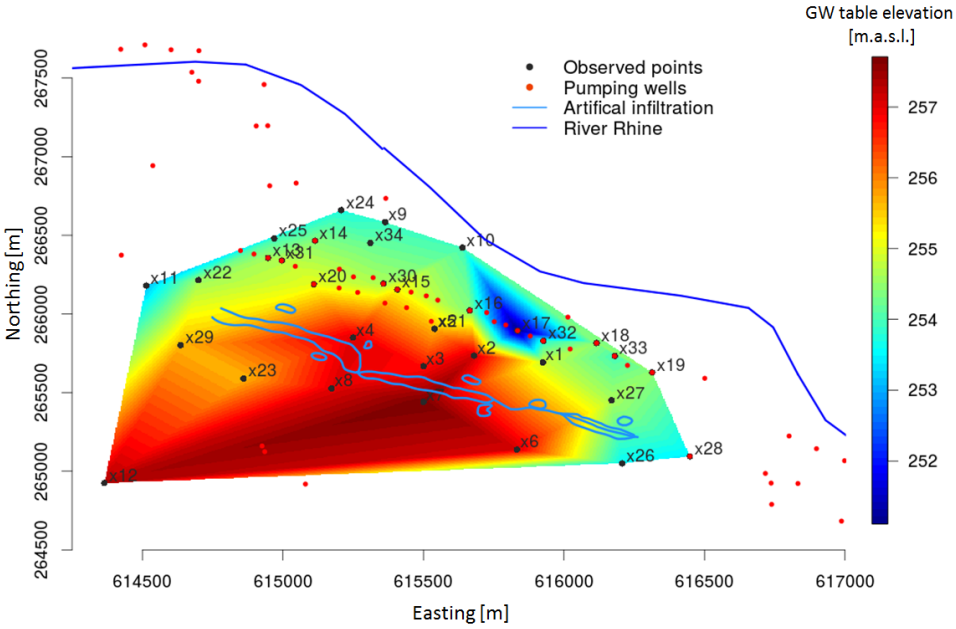

Figure 3.3: Linearly interpolated water table elevations from 34 observed points in March 2015.

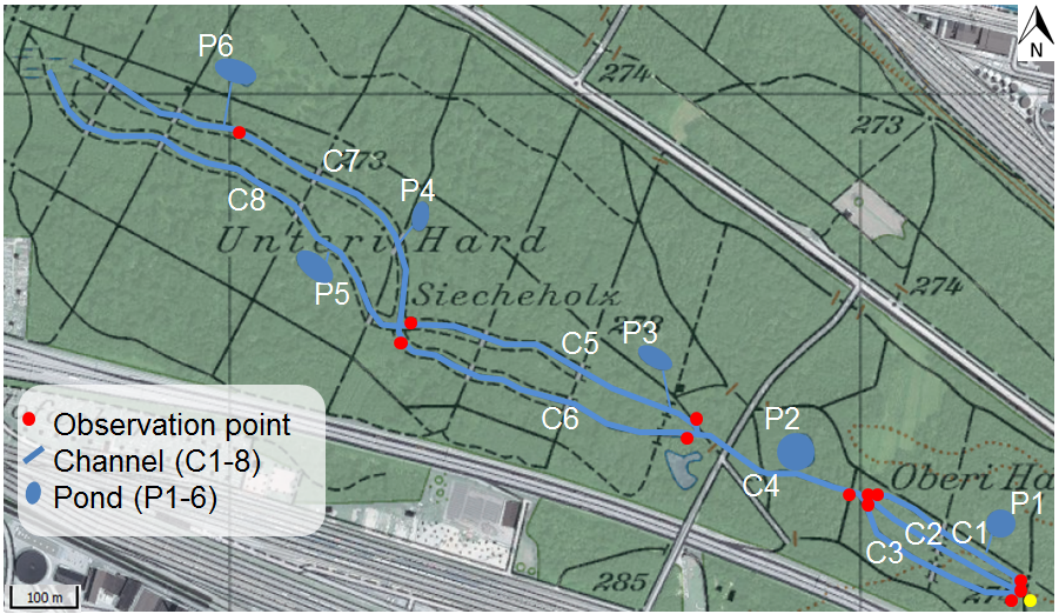

Figure 3.4: Infiltration channels and ponds with observation points for discharge and water level measurements. All water is entering the infiltration system at the yellow marking point.

on, we will refer to the heads of the channels as "water levels", to have a better distinction between surface water- and groundwater-heads. Figure 3.4 shows the observation points as well as the individual labeling of every channel segment.

We used the OTT MF Pro device, which measures flow velocity and water levels with an electromagnetic current meter. With the measured parameters it automatically computes discharge based on USGS and ISO methods (OTT, 2012).

Additionally, employees of the Hardwasser AG measured the water levels at the same spots weekly. Hence, a time series of water level data from August 2008 to January 2013 is available. These data are shown in Figure 3.5 illustrating that in some segments the mean water outflow is higher than the mean water inflow, which is the case in channels 1, 3, 6 and 7. This is due to the fact that channels with higher water levels are loosing water to neighboring channels with lower water levels. This results in higher water levels at the outflow than the inflow of the gaining stream. This phenomenon is later demonstrated by our numerical modeling (see Section 5.2.5).

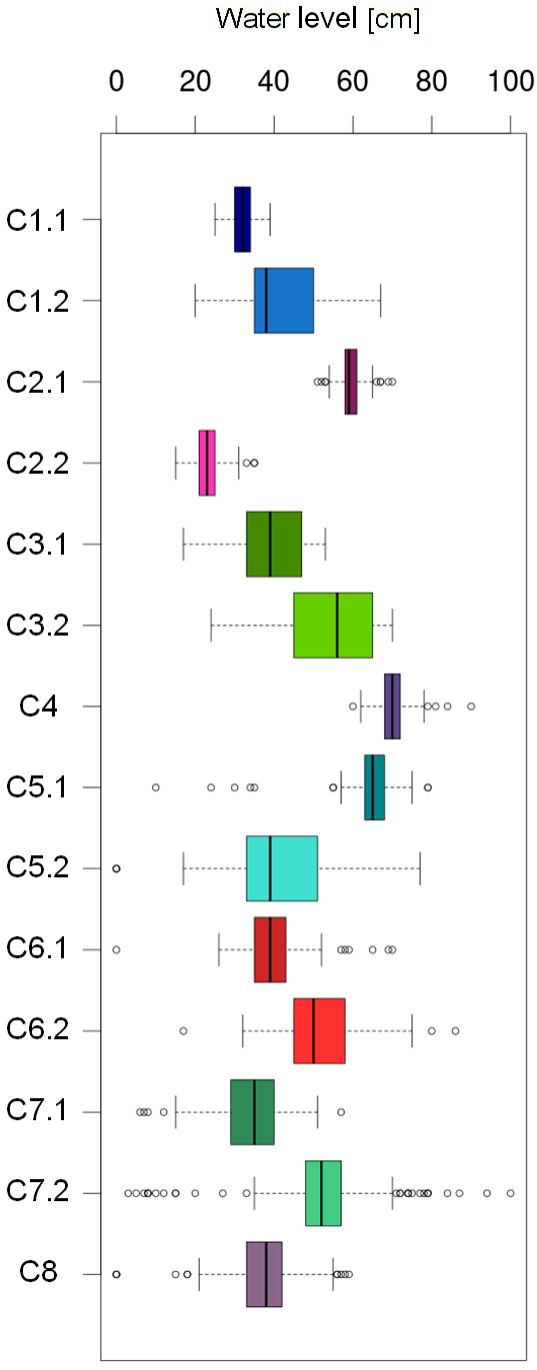

Figure 3.5: Variance of water levels of each observation point (Cx.1 represents the water inflow, Cx.2 the water outflow of each channel segment; there are no outflow observation points for channels 4 and 8).

4

Estimation of Spatial and Temporal Infiltration

Based on existing and recently obtained discharge and water level data, we were able to estimate the spatial and temporal infiltration.

4.1 Rating Curves

By means of rating curves the water level time series were converted to discharge. Rating curves define the relationship between water level and discharge (WMO, 2008). In this study, we applied a nonlinear power-law model, which is based on the equation

$$Q = A(h + c)^b \tag{4.1}$$

where Q [m^3/d] is the discharge, h [m] is the channel water level and A, b, c [$-$] are calibration coefficients. Equation 4.1 is the most widespread and recommended formula for describing the water level-discharge relationship and has been applied at gauging stations worldwide (Reitan and Petersen-Øverleir, 2004; Petersen-Øverleir, 2005).

Figure 4.1 exemplifies an established rating curve for the observation point at the water inflow of channel 4. This example demonstrates that the observations were all taken within a relatively small range. Given that the water inflow at the study site is controlled artificially, it is difficult to measure extreme events.

The established rating curves for each channel segment have a sufficient coefficient

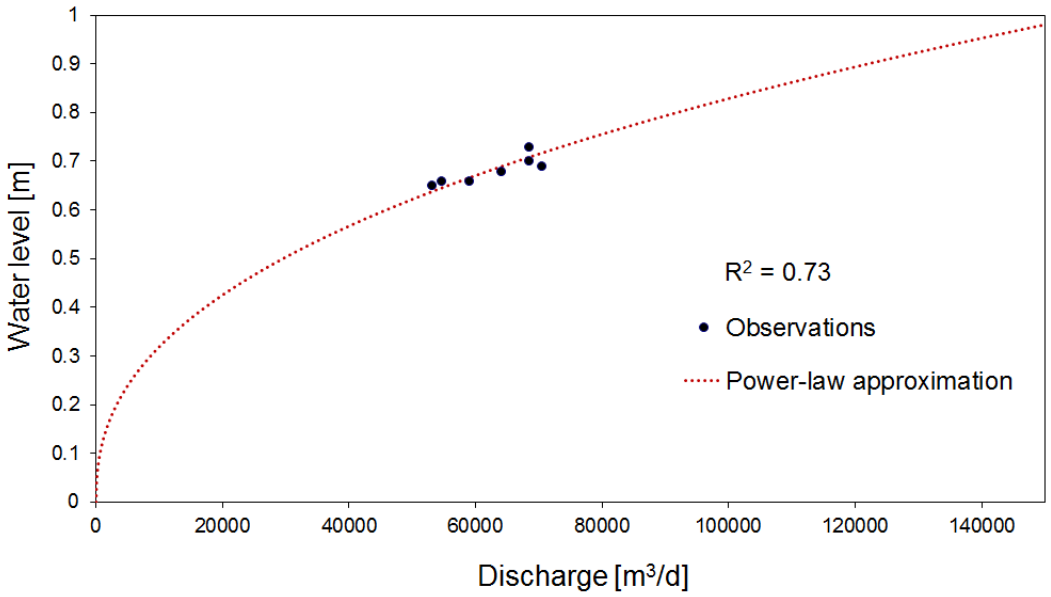

Figure 4.1: Example of a stage-discharge rating curve at the water inflow point of channel 4.

of determination (R^2), which ranges from 0.70 to 0.99 (except for the outflow of channel 3, which has an R^2 of 0.26 due to an insufficient number of observations).

4.2 Calculation of Infiltration Rates

Next, we determined the infiltration of each channel segment by assuming that the infiltration equals the water inflow minus the water outflow. For the channels connected to ponds, we substracted the water amount flowing into the ponds. Our approach is summarized by the following equation:

$$Infiltration = channel\ inflow\ (-pond) - channel\ outflow \tag{4.2}$$

The data of the water flowing into to ponds were provided by the Hardwasser AG. All water flowing into the ponds is infiltrating there. Evapotranspiration and precipitation were not considered since the amount of river water infiltrating into the system is about two orders of magnitude higher than natural infiltration. Hence, we assume that these two parameters have no significant impact on the estimation of infiltration rates.

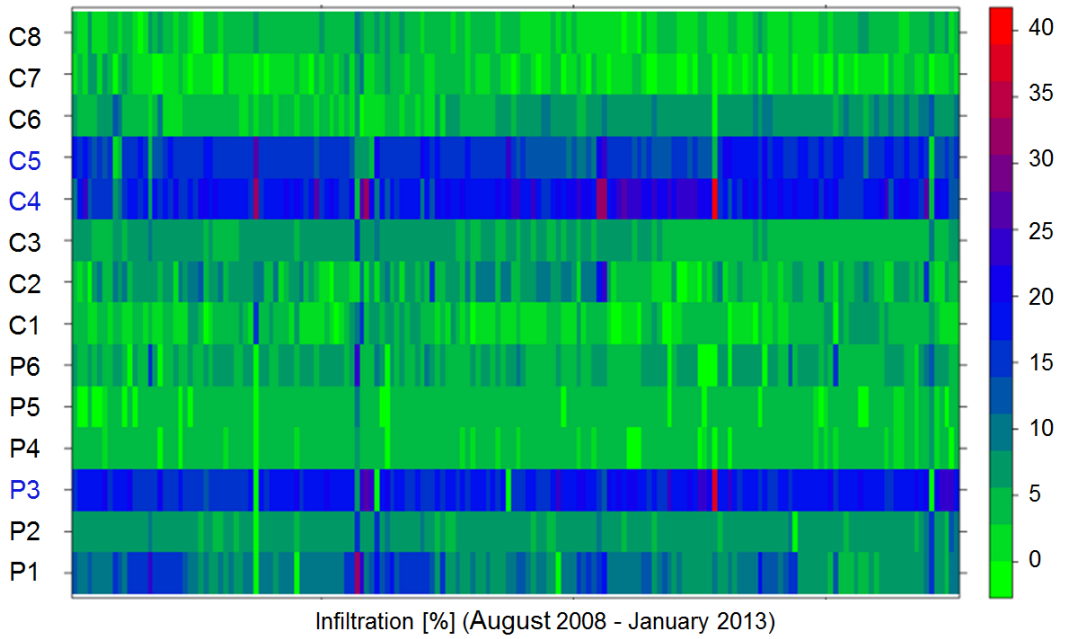

Figure 4.2: Relative infiltration of each channel (C1–8) and pond (P1–6) showing the highest infiltration rates at channels 4 and 5, and pond 3.

Table 4.1: Reach lengths, mean water levels and mean infiltration rates of each channel (C1–8), and pond areas and mean infiltration rates of each pond (P1–6). *) Note that pond areas are approximated.

	C1	C2	C3	C4	C5	C6	C7	C8
Reach length [m]	312	304	325	277	531	549	717	656
Mean water level [cm]	33	36	42	47.5	46.5	40	17	15
Infiltration [%]	1	5	6	19	14	6	1	3
Infiltration [m^3/d]	1 706	7 582	8 804	29 119	22 361	8 798	1 849	4 389

	P1	P2	P3	P4	P5	P6
Pond area*) [m^2]	835	2449	2208	785	1634	2334
Infiltration [%]	10	7	171	3	3	6
Infiltration [m^3/d]	15 429	10 255	10 412	4 050	4 202	8 404

4.3 Results and Discussion

Using the provided and observed data, we were able to establish rating curves, and thereby determine the spatial and temporal infiltration for every segment of the infiltration system for the given time series.

Thus, we could identify the segments with the highest infiltration rates. Figure 4.2 illustrates the relative contribution of each channel and pond to the total infiltration rate. The blue segments have the highest infiltration rates, which appear in channel 4 (19%) and 5 (14%), and in pond 3 (17%). The segments in green contribute

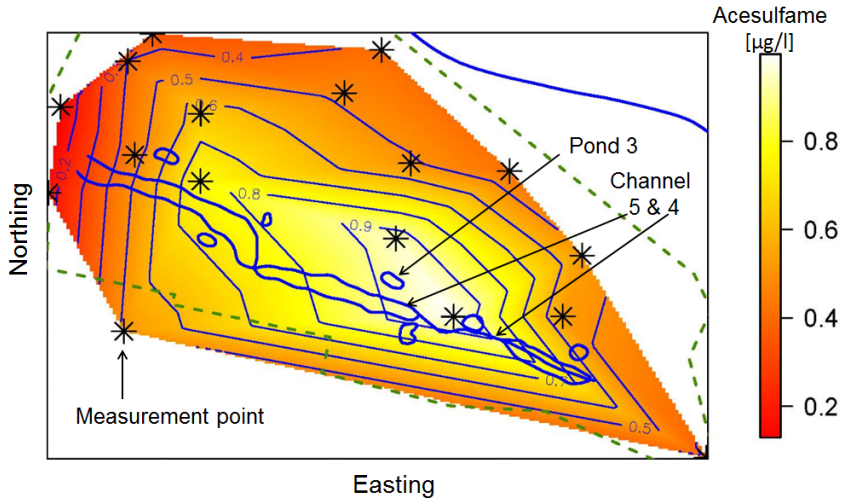

Figure 4.3: Linearly interpolated observations of acesulfame, an artificial sweetener, and trace substance originating from the river Rhine.

with 1 to 10 percent to the total infiltration rate. These findings match the data in Table 4.1, which shows that channels 4 and 5 have either a long reach length, the highest mean water level, or both.

Additionally, these results accord with earlier measurements of the trace substance acesulfame (data were provided). Acesulfame is an artificial sweetener originating from the river Rhine. Since river water is the input source for the infiltration, we assume that the highest accumulation of acesulfame correlates with the highest infiltration rates. The highest concentrations of acesulfame are close and further downstream to the area of the highest infiltration rates as illustrated in Figure 4.3. Figure 4.2 also shows that the temporal infiltration for the analyzed time series is relatively stable. Hence, water level fluctuations as later shown in Figures 4.4 and 4.5 do not significantly influence the infiltration rate.

Figures 4.4 and 4.5 exemplify the water inflow and outflow of channel 5 and 6. They also show the fluctuations of the incoming and out flowing water, respectively. The trends illustrated by linear regressions in Figures 4.4 and 4.5 show that there is a slight decrease of discharge for the available time series. However, the mean discharge rate is relatively stable. On average channel 5 loses about 86% of its water from the inflow to the outflow. This is because about 30% of water is flowing off to pond 3 where it entirely infiltrates. Additionally, there are higher water levels in channel 5 resulting in higher infiltration rates. Compared to that, channel 6 with

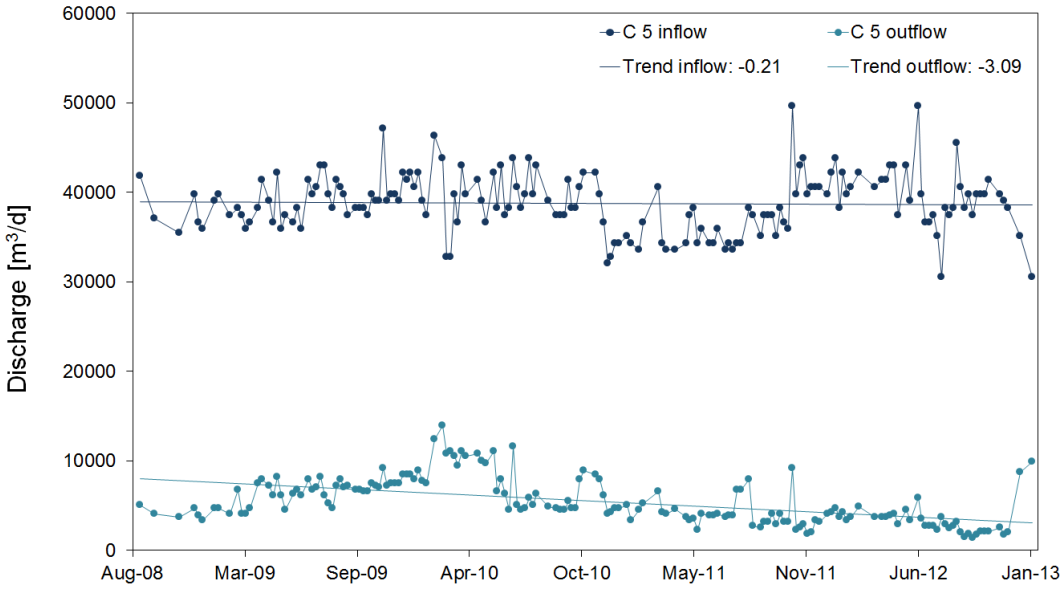

Figure 4.4: Water inflow and outflow of channel 5 with linear regression trends (August 2008 – January 2013).

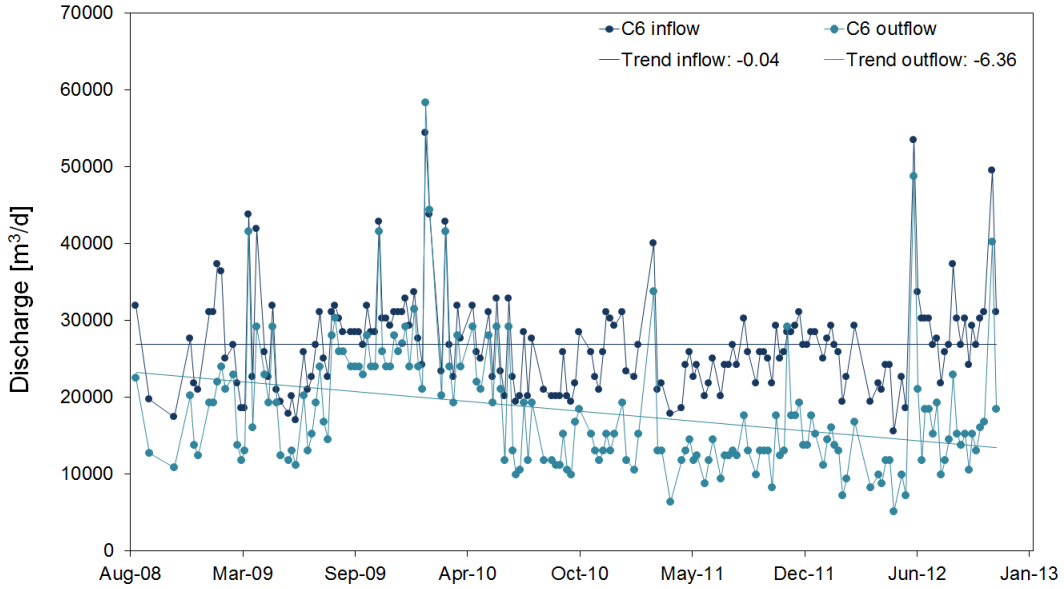

Figure 4.5: Water inflow and outflow of channel 6 with linear regression trends (August 2008 – January 2013).

no connection to any pond and lower mean water levels compared to channel 5 loses only 22% of water.

Combining all estimations, a total mean infiltration of about 135 000 m^3/d was calculated. The Hardwasser AG records the water inflow into the system, which has a mean value of about 96 000 m^3/d. The histogram in Figure 4.6 shows the devia-

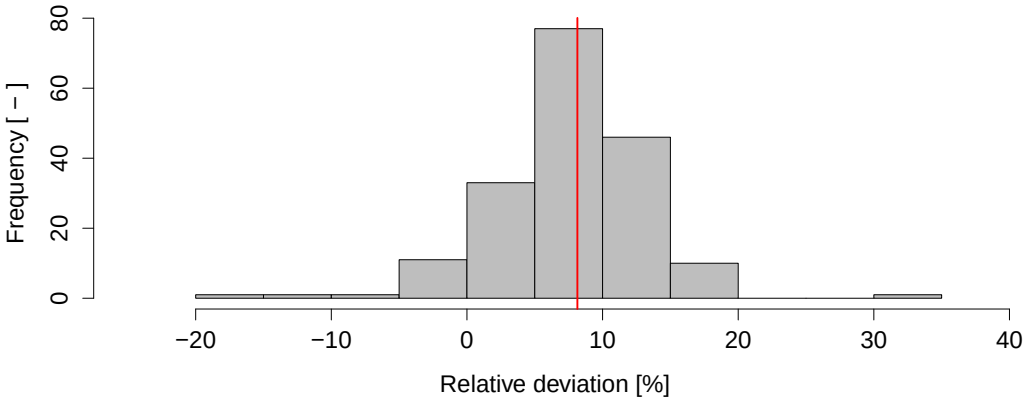

Figure 4.6: Deviation (in percent) between the total measured inflow (provided data by the Hardwasser AG) and the total estimated inflow (sum of the calculated water inflow at the first three points via rating curves); the red line marks the mean deviation of 8%.

tion (in percent) between the estimated total inflow and the observed total inflow measured by the Hardwasser AG. The histogram shows that the estimated inflow is higher than the measured one with a mean deviation of +8%. This uncertainty could be a result of a combination of factors such as an insufficient number of observations or equipment and reading errors. However, the results are reasonably consistent with previous studies (Affolter et al., 2010; Matousek et al., 2011) and serve as an adequate basis and comparison for the subsequent numerical modeling.

5

Numerical Modeling

For this thesis, the physically-based modeling code "HydroGeoSphere", developed by René Therrien, has been selected (Therrien et al., 2010). HydroGeoSphere is a fully-coupled modeling software, which is well established for simulating three-dimensional (3D), variably-saturated subsurface flow. Additionally, HydroGeoSphere accounts for all components of the hydrologic cycle and is capable of simulating the build-up of groundwater mounds beneath streams, which is an important aspect for our model domain (Brunner and Simmons, 2012).

5.1 Governing Equations of HydroGeoSphere

The underlying equations of HydroGeoSphere are briefly summarized in this section. In Therrien et al. (2010) a more precise description is given.

HydroGeoSphere uses the following modified formulation of the Richards's equation for describing 3D transient subsurface flow in a variably-saturated porous medium:

$$\frac{\partial(S_w\theta_s)}{\partial t} - \nabla \cdot (Kk_r\nabla h) = \Sigma\Gamma_{sub} \pm Q \tag{5.1}$$

where S_w [$-$] represents the degree of water saturation, θ_s [$-$] is the saturated water content, which is assumed to be equal to the porosity, t [d] denotes the time, K [m d^{-1}] is the saturated hydraulic conductivity tensor, k_r [$-$] is the relative permeability, h [m] is the hydraulic head, Γ_{sub} [d^{-1}] is the fluid-exchange rate, and Q [m d^{-1}] represents the external sources or sinks outside the model domain.

In addition to equation 5.1, the relationships between the hydraulic heads, the rel-

ative permeability and the water saturation are needed for simulating unsaturated flow. Hence, the saturation-pressure relationship based on the work of Mualem (1976) and later proposed by van Genuchten (1980) was used:

$$S_w = S_{wr} + (1 - S_{wr})[1 + |\alpha\psi|^{\beta}]^{-\nu} \quad \text{for } \psi < 0$$
$$S_w = 1 \quad \text{for } \psi \geq 0$$

with the relative permeability given by:

$$kr = S_e^{(l_p)} \left[1 - \left(1 - S_e^{1/\nu}\right)^{\nu}\right]^2 \tag{5.2}$$

with

$$\nu = 1 - \frac{1}{\beta}, \quad \beta > 1 \tag{5.3}$$

where S_{wr} $[-]$ is the residual water saturation, α $[m^{-1}]$ and β $[-]$ are parameters obtained by fitting experimental results to Equation 5.3, ν $[-]$ represents another fitting parameter, ψ $[m]$ is the pressure head and l_p $[-]$ the pore-connectivity parameter, which was estimated to be 0.5 for most soils by Mualem (1976).

5.2 Cross-Section Model

We set up a steady state model to investigate the interactions of the channels and the groundwater. The aim was to identify the sensitivity of the system to certain key factors governing the infiltration. Stream water levels, aquifer and clogging layer properties, and the depth to the groundwater table were in earlier studies identified to have a string impact on infiltration rates (Winter, 1999; Woessner, 2000; Cardenas, 2009; Brunner et al., 2009a, 2011; Doble et al., 2012; Morel-Seytoux et al., 2014; Rivière et al., 2014). Hence, these parameters were investigated with the following model.

5.2.1 Model Setup

As shown in Figure 5.1, the model domain is 212 m wide, 549 m deep and 51.5 m high. We implemented two rectangular channels underlain by a confined streambed, which is from now on referred to as clogging layer (CL). The aquifer beneath the channels is 50 m thick. Although the thickness of the clogging layer is unknown, we

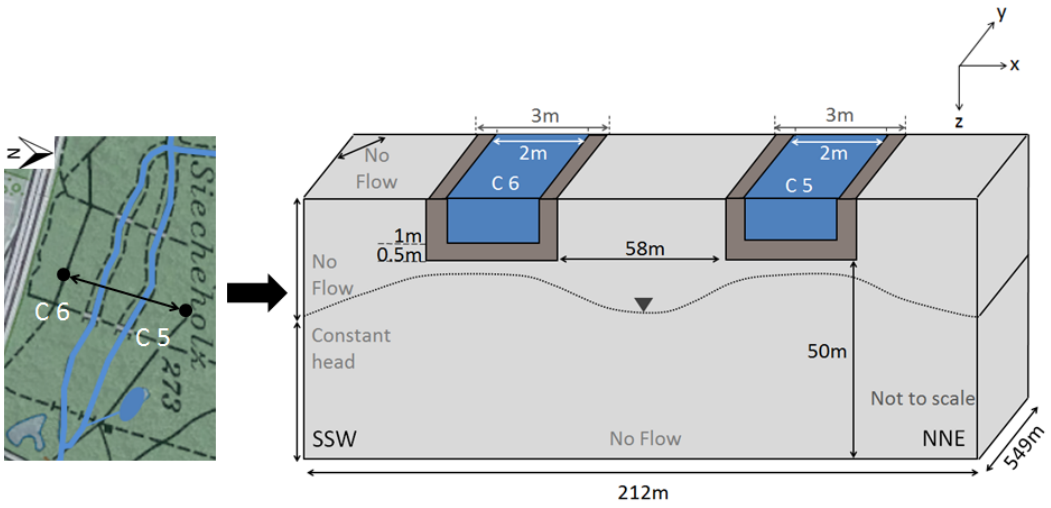

Figure 5.1: Segment of channels 5 and 6 of the study area (left). Model domain and boundary conditions representing the selected segment (right).

assumed it to be 0.5 m. This clogging layer thickness was initially chosen according to the findings of Fox and Durnford (2003) and later investigated in the second sensitivity analysis. The lateral model boundaries have a distance of 76 m to each channel. We also investigated the impact of further increasing the distance of the boundaries on the infiltration flux. However, larger distances from the streams resulted in no significant differences in infiltration rates (see appendix A). We assigned constant head boundaries to the channels and to the lateral model boundaries. For the latter, we used the values of observed groundwater table elevations from the closest observation wells (black points in Figure 5.1).

In a simplified form this cross-section represents channels 5 and 6 as indicated in Figure 5.1 (left panel), since all dimensions of the model domain are according to this segment of the study site. The pond, which is connected to channel 5, was not taken into account, since the primary aim of this model was to investigate the sensitivities of the channels and interactions between them. Furthermore, we did not consider precipitation and potential evapotranspiration. These parameters have a negligible influence on the infiltration flux of the model considering the preternatural amounts of water entering the system.

Furthermore, there is a slope of 0.5 m from channel 6 to channel 5 (channel 5 is located further north), which was considered in the model set up by placing the head boundary of channel 5 0.5 m below channel 6.

Table 5.1: Soil types and characteristics according to van Genuchten's model for unsaturated conditions (α [m^{-1}]: parameter in the soil water retention function; β [−]: exponent in the soil water retention function; K_s [m d^{-1}]: saturated hydraulic conductivity) (Carsel and Parrish, 1988).

Model domain	Material	α [m^{-1}]	β [−]	K_s [m d^{-1}]
Aquifer	Sand	14.50	2.68	1.00
Clogging layer	Loam	3.60	1.56	0.07

This idealized system assumes the aquifer and clogging layer material to be isotropic and homogeneous. First, we used typical van Genuchten parameters and saturated hydraulic conductivities (K_s) values for sand (aquifer) and loam (clogging layer) (Carsel and Parrish, 1988). Table 5.1 shows the exact values. The model setup was adapted from Irvine et al. (2012).

All simulations were run using the 3D variably-saturated HydroGeoSphere code. First, the necessary data files for the pre-processor file (grok) were written. These contain the discretisation of the grid structure, the definition of the material properties and the flow boundary conditions. The grok file implies instruction-driven text and generates input data files for HydroGeoSphere. After running HydroGeoSphere, output data files are created. The postprocessing was done using HSPLOT, which converts the output data (binaries) to ASCII files. The latter can be imported by Tecplot, a third-party visualization software for numerical simulations (Therrien et al., 2010; Tecplot, 2013). An example input file for this model is appended.

5.2.2 Sensitivity Analysis I — Water Levels

We conducted a first sensitivity analysis to investigate the flow field between the two channels. Two main factors might influence the flow field: (i) the regional gradient of about 0.5 m from channel 6 to channel 5, and (ii) the constantly higher water levels of channel 5 compared to the ones of channel 6 (except for very few cases within the given time series).

The water levels of each channel are within the range of 40 cm to 49.75 cm for channel 6, and within 48 cm to 59 cm for channel 5 (lower and upper quartile). Figure 5.2 illustrates the distribution of the water level data of channel 6 (left) and 5 (right).

To investigate a standard operating mode, we set the median water level values of

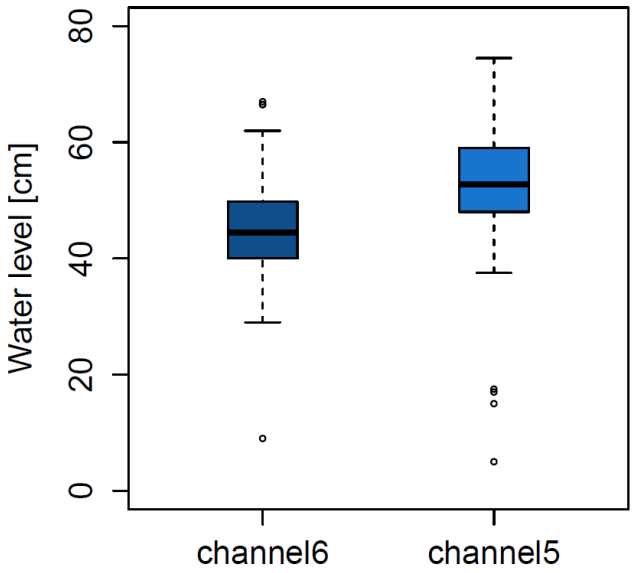

Figure 5.2: Mean water levels (average of channel inflow and outflow water levels) of channel 6 (left) and channel 5 (right) (August 2008 – January 2013).

each channel as constant head boundaries to simulate the flow field.

The Hardwasser AG tries to guarantee a stable infiltration rate by keeping constant water levels. However, as shown in Figure 5.2, the water levels vary, for example if there is a construction on certain segments. During such incidents, it may happen that there is almost no water flowing in one channel and hence, most of the water is flowing through the other channel. To investigate the influence of such extreme water levels, we simulated two cases where (i) 80% of the water is flowing in channel 5 and the remaining 20% of the water is flowing in channel 6, and (ii) vice versa.

5.2.3 Sensitivity Analysis II — Clogging Layer and Depth to the Water Table

We used the subsequent sensitivity analysis to compare the modeled to the estimated infiltration rate. Here, the most influential factors besides the water levels were analyzed: the depth to the water table and the clogging layer thickness.

Knowing the hydraulic connections between a stream and the underlying aquifer is crucial for water resources management. Principally, there are two fundamentally different flow regimes: the stream drains the aquifer (gaining stream) or the stream replenishes the aquifer (losing stream) (Brunner et al., 2009a). The head difference

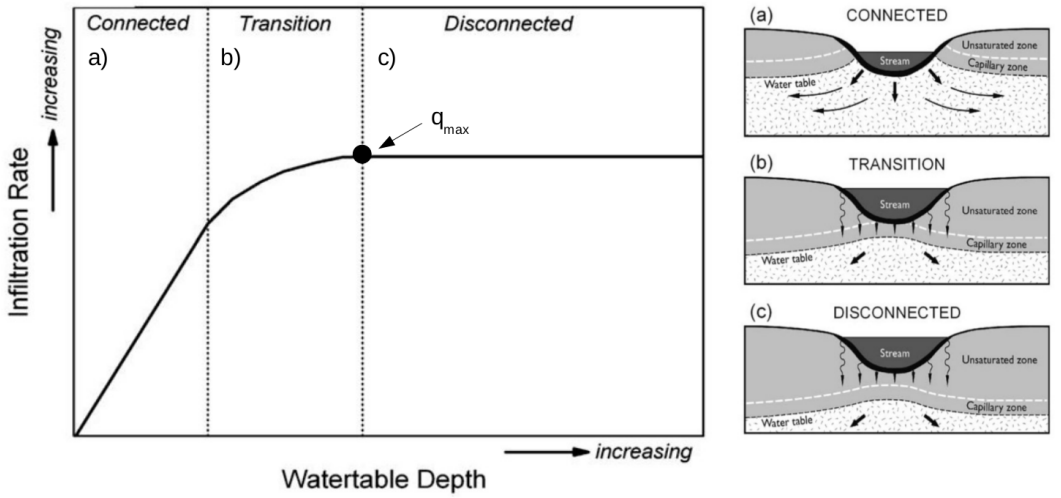

Figure 5.3: Schematic diagram of an infiltration curve showing changes in infiltration as a function of the water table depth (left). Brunner et al. (2009a) identified three different flow regimes: a) the infiltration rate increases linearly by increasing the depth to the water table, b) further lowering of the water table leads to a transition stage where the infiltration rate is no longer a linear function of the head difference and c) point q_{max} is reached where the groundwater table is sufficiently far below the stream and further changes in the depth to the water table do not significantly affect the flow rates. Figure adapted from Brunner et al. (2009a).

between the two compartments (from now on referred to as depth to the water table) determines the flow regime.

Previous studies detected that the zone beneath a stream becomes unsaturated when the depth to the groundwater table reaches a certain distance below the clogging layer (Osman and Bruen, 2002; Fox and Durnford, 2003; Bruen and Osman, 2004; Brunner et al., 2009a,b; Irvine et al., 2012).

When the water table is initially lowered, it causes a linear increase of the infiltration flux. The stream and the aquifer are still connected (see Figure 5.3a). Further lowering of the water table causes the seepage through the aquifer to become faster than the replacement through the clogging layer. The increasing depth to the water table leads to an increase of the hydraulic gradient. Hence, the aquifer material begins to desaturate. At this point, there is a non-linear relationship between infiltration flux and the depth to the water table. The system is in transition from a connected to a disconnected state, as shown in Figure 5.3b. Eventually, further lowering of the water table has no significant influence on the infiltration flux anymore. A constant value (q_{max}) has been approached and the stream is said to be disconnected accord-

ing to Brunner et al. (2009a) (see Figure 5.3c). However, this term should not be mistaken for a lack of interaction between surface and groundwater (Fleckenstein et al., 2006).

Another controlling factor for infiltration is the clogging layer thickness. Clogging layers are less permeable than the natural soil material and thus reduce the infiltration rate. For these reasons, we modeled infiltration rates for different clogging layer thicknesses from zero to half a meter as a function of the depth to the water table. To simulate the effects of clogging layers with a thickness of a few centimeters, a refinement of the initial model discretisation was necessary.

5.2.4 Sensitivity Analysis III — Saturated Hydraulic Conductivity

With the help of the results of the second sensitivity analysis, we adjusted the clogging layer thickness to a more legitimate value. However, even with the adjusted clogging layer thickness there still existed a difference between the modeled and the previously estimated infiltration rates. Hence, we conducted a third sensitivity analysis to vary the saturated hydraulic conductivity of the aquifer and the clogging layer, since the K_s values are another key factor influencing the infiltration rate (Brunner et al., 2009a).

For this analysis, PEST, a model-independent parameter estimation tool coupled with HydroGeoSphere, was used to automatically calibrate the K_s values (Doherty, 2010).

5.2.5 Results and Discussion

With the first sensitivity analysis, the impact of the water levels on the flow field was investigated. Figure 5.4 illustrates the flow field and potential water heads for the mean observed water levels of each channel. The stream traces indicate that under standard operating conditions all water originating from channel 6 is flowing south (SSW). This was later proven by the 3D model (see Section 5.3). The infiltrated water of channel 5 flows partially towards channel 6 as well as to the north. The fact that the water is flowing in both directions (SSW and NNE) shields the study site from potentially contaminated water from the surrounding area. Furthermore, these results explain the higher water levels at the outflow of channel 6, since water

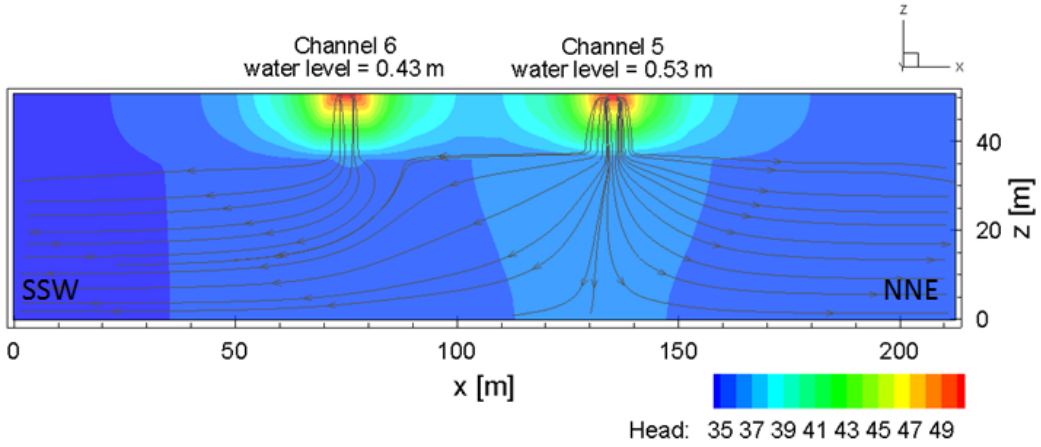

Figure 5.4: Mean observed water levels of channel 5 and 6 (August 2008 – January 2013).

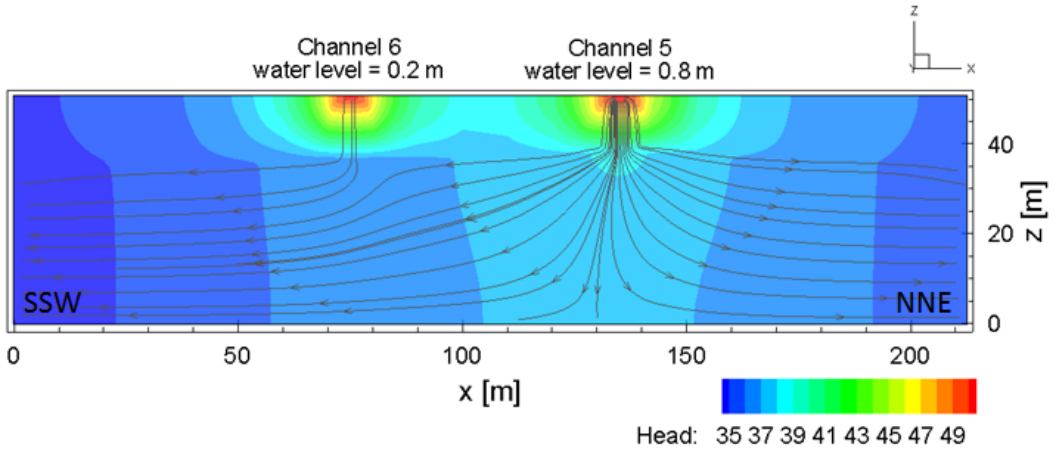

Figure 5.5: First extreme case with 0.2 m water level in channel 6 and 0.8 m water level in channel 5.

is flowing from channel 5 to channel 6 due to the higher water level in channel 5.

Next, we examined two extreme cases with 20% of the water flowing in channel 6 and 80% in channel 5, and vice versa. The flow fields of these simulations are shown in Figures 5.5 and 5.6, respectively.

The stream traces and groundwater heads of the first extreme case of 0.2 m water level in channel 6 and 0.8 m water level in channel 5 (assuming a total water depth of 1 m), illustrated in Figure 5.5, show no considerable difference in the flow field compared to the standard operating mode (Figure 5.4).

Figure 5.6 presents the flow field for the second extreme case with 0.8 m water level in channel 6 and 0.2 m water level in channel 5. For this case the stream traces

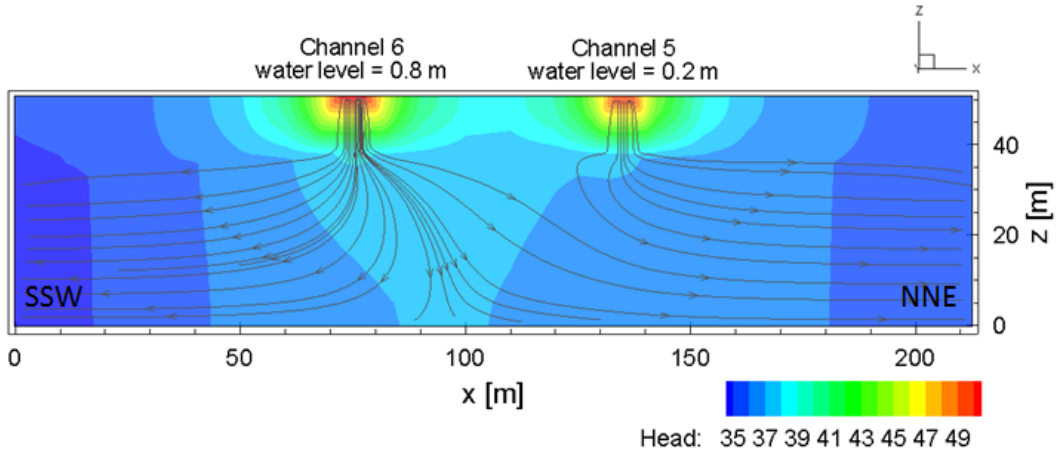

Figure 5.6: Second extreme case with 0.8 m water level in channel 6 and 0.2 m water level in channel 5.

indicate that there is water flowing from channel 6 to channel 5. This did not occur in the two previously investigated cases.

The extreme cases show that a change of the water levels within a feasible range may result in a partial change of the flow direction in the second extreme case. However, for all cases the water of the two channels distributes in both directions (SSW and NNE). Therefore, we concluded that the hydraulic barrier is still intact even for extreme water levels.

With the second analysis, we were able to identify the sensitivity of the system to both the depth to the water table and the clogging layer thickness. Figure 5.7 shows infiltration rates as a function of the clogging layer thickness and the depth to the water table. The vertical red line represents the average depth to the water table at the study site, which is about 16 m. The yellow points represent q_{max} for every specific curve, where the highest infiltration rate, and accordingly a disconnected flow regime is reached.

The results of this analysis support the theory developed by Brunner et al. (2009a), who demonstrated that the depth to the water table has a significant impact on the infiltration rates. Subsequently, we were able to determine the flux regime with this approach, which proves to be disconnected for the underlying depth to the water table. Figure 5.8 illustrates the saturation for standard operating conditions of the first sensitivity analysis and shows the existence of an unsaturated zone beneath the channels for the given conditions.

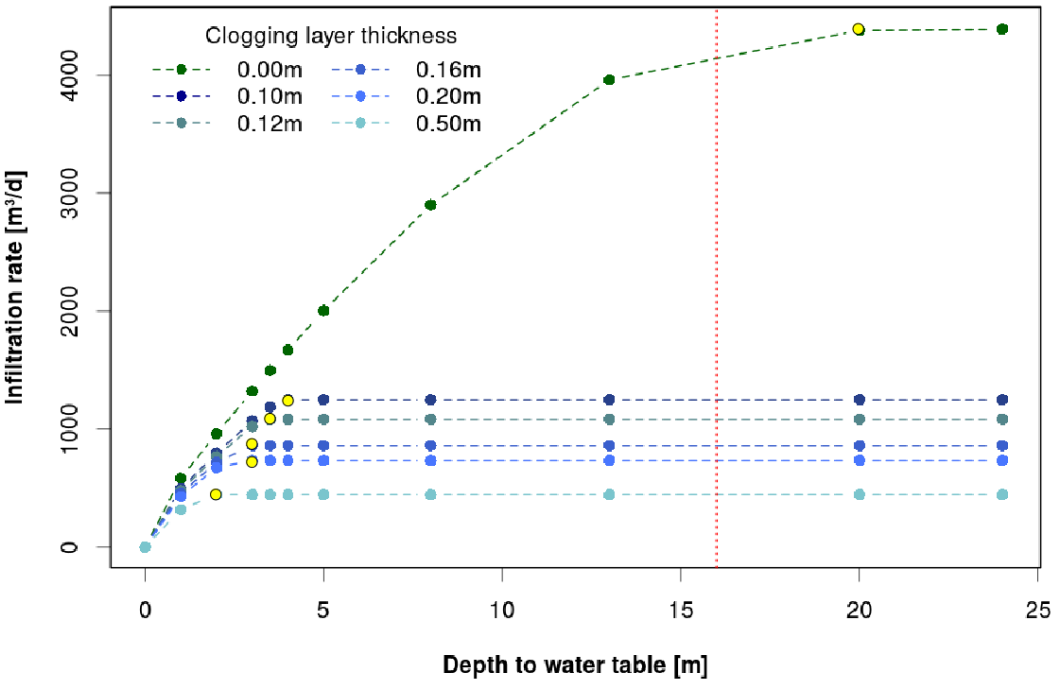

Figure 5.7: Infiltration fluxes with no clogging layer and different clogging layer thicknesses (0.1 m–0.5 m) as a function of the depth to the water table and with constant head boundaries of 0.5 m at both channels. The red line marks the average depth to the water table (16 m) at the study site. The yellow points highlight q_{max}, the point where the highest infiltration rate is reached.

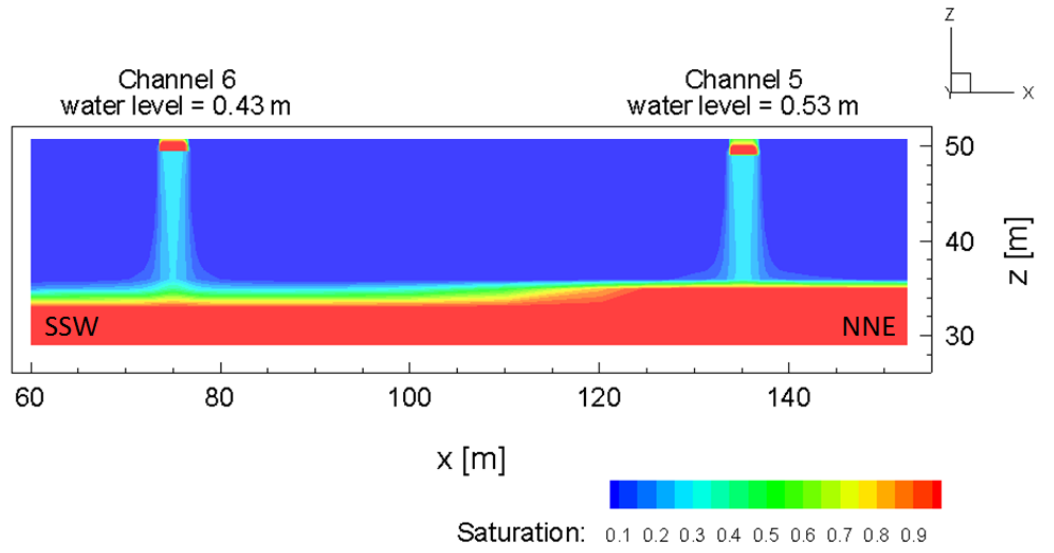

Figure 5.8: Saturation for mean water levels in channels 6 and 5. The unsaturated zone beneath the clogging layer proving the state of disconnection.

Table 5.2: Calibrated K_s values for the clogging layer and aquifer material.

Model domain	Material	K_s [m d^{-1}]
Aquifer	Gravel	78.30
Clogging layer	Sandy loam	1.34

As mentioned above, the clogging layer thickness at Hardwald is unknown. By comparing the modeled infiltration rate of about 500 m^3 d^{-1} (for a clogging layer thicknesses of 0.5 m; see Figure 5.7) to the estimated infiltration of 26 200 m^3 d^{-1} (summarized value for mean water levels at channels 5 and 6), we concluded that the initial clogging layer thickness of 0.5 m had to be adjusted to a thinner clogging layer. This assumption also goes along with the fact that the infiltration system gets excavated every five to ten years, preventing the formation of a thick clogging layer. Additionally, the river water is put in settling tanks and gets filtered before the infiltration. After this treatment, 95% of all suspended matter of the raw water is filtered. However, even if the input water has a low concentration of suspended matter, erosion and deposition (Hatch et al., 2010), and biological activities (Treese et al., 2009) might change and clog the streambed material over time. Hence, we concluded that a rather thin clogging layer of about 0.1 m is most likely.

With an adjusted clogging layer thickness of 0.1 m the simulated infiltration rate was about 1 600 m^3 d^{-1}, which is an order of magnitude below the estimated one based on the rating curves of 26 200 m^3 d^{-1}. Hence, we conducted a third analysis where we calibrated the K_s values for the clogging layer and the aquifer materials. The results from this calibration are shown in Table 5.2. The calibrated saturated hydraulic conductivity for the aquifer material is almost 80 times higher than the initial one. The K_s value for the clogging layer was calibrated to be 19 times higher than the primary one. The new values conform to literature data for a sandy-gravel aquifer material and a sandy-loam clogging layer material (Stephens, 1976). With the calibrated values we were able to simulate a total infiltration for channels 5 and 6 with mean water levels of 26 000 m^3 d^{-1}.

The sensitivities of each investigated parameter are summarized in Table 5.3 showing that all parameters have a strong influence on the infiltration rates. For the investigation of the influence of water levels in infiltration rates see appendix A.

However, the applications of this cross-section model are limited, since it is highly

Table 5.3: Evaluation of the impact of the investigated parameters on the infiltration rates.

Controlling factor	Impact	Manageable
Water level	high	yes
Depth to the GW water table	high (till disconnection state is reached)	conditionally
CL thickness	high	yes
CL and aquifer properties	high	no

simplified and only serves as a tool to identify the sensitivities of the system. A key limitation factor of this model is the fact that the hydraulic conductivity and the thickness of the clogging layer are not known. Additionally, the findings about the clogging layer properties should be taken with caution, since previous studies suggested that streambeds are highly heterogeneous (Calver, 2001; Irvine et al., 2012). The assumption of a homogeneous geological structure can lead to a model error of up to 34%. However, Irvine et al. (2012) pointed out that the results are accurate even with a clogging layer assumed to be homogeneous if the calibration and prediction are made for the same flow regime, which is the case in this study.

5.3 3D Model

The previous cross-section model helped to develop a sound understanding of the most influential impacts on infiltration and the interactions between the channels. To understand how the entire system is reacting under different operating conditions, we developed a new 3D model representing the entire study area.

5.3.1 Model Setup

A new grid was built with "GRID BUILDER", a 2D triangular finite element grid generator developed by Mc Laren (2011). The geometries are based on ArcGIS files since GRID BUILDER can handle georeferenced data. Finally, we implemented the 2D grid in HydroGeoSphere and extended it to a 3D grid by adding ten extra layers. The top layer includes a digital elevation model with a resolution of 25 meters.
For the lateral boundaries in the south and the west of the model domain, we assigned linearly interpolated groundwater table elevations observed in the March 2015 field campaign. The lateral boundaries in the east represent linearly interpolated data of water levels from the river Rhine (data were provided by the waterworks).

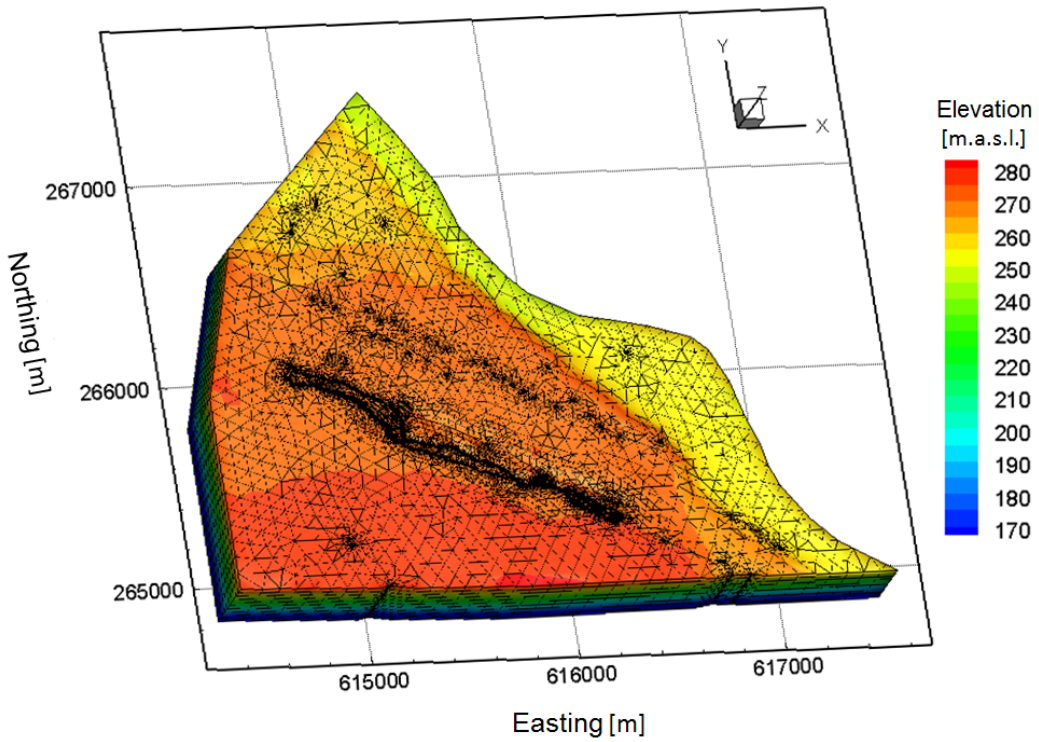

Figure 5.9: 3D model domain showing the distribution of elevation in the study area Hardwald.

We included the infiltration system with all ponds and channels as well as the pumping wells (Hardwald pumping well gallery and industrial wells) and observation wells. A finer grid discretisation was used around the infiltration system and the pumping wells. The infiltration rates were assigned as specified fluxes based on the estimated infiltration. Thus, we had to convert the infiltration rates estimated in m^3 d^{-1} to m d^{-1} by dividing through the area of the channels. The clogging layer was neglected, since the specified flux is based on the estimated infiltration rates, which already implies the clogging layer. The calibrated K_s value was assigned to the aquifer material, which is assumed to be isotropic and homogeneous. An example input file for this model is appended.

Figure 5.9 shows the model domain with the elevation distribution in the study area. The highest elevations are in the south-western part. The lower elevations towards the river illustrate the Rhine rift. Furthermore, it shows the finer grid discretisation around the infiltration system and the pumping wells.

The model runs in a saturated steady state mode and was used to simulate the total

infiltration of all segments, the groundwater table elevations and the build-up of a groundwater mound. Later, we used scenario modeling to simulate different water injection and abstraction rates to investigate the effect on the groundwater mound and the fluxes in the study area.

5.3.2 Scenario Modeling

The results of the modeled groundwater table elevations suggested that the built groundwater mound at the last segments might not be sufficient to prevent the inflow of contaminated water. Hence, the aim of the scenario modeling was to simulate higher groundwater table elevations close to the last segments (channels 7 and 8, and ponds 4 and 5) of the infiltration system. Therefore, we used three different scenarios. For the first scenario we increased the specified flux of channels 7 and 8, and ponds 4, 5 and 6 by about 20%. This was done to check if an increased flux of 20% would already lead to higher groundwater table elevations on the last segments. Following the results of the first scenario, the fluxes at the same segments were doubled. This scenario was conducted to test the sensitivity of the system to increased fluxes. Finally, in the last model scenario we used the conditions of the first scenario combined with pumping rates cut by half at the western wells to investigate the influence of a combined approach of reduced groundwater pumping and increased fluxes.

5.3.3 Results and Discussion

This 3D model simulated a total infiltration flux of 92 200 m^3 d^{-1}. The simulated total infiltration depends on the chosen segments in GRID BUILDER and is based on the estimated infiltration data.

The simulated groundwater table elevations are shown in Figure 5.10. The elevation distribution is consistent with the previously shown distribution of observed groundwater table elevations from the March 2015 field campaign (see Figure 3.3). Comparing the observed to the modeled groundwater table elevations, there is a fit of an R^2 of 0.8 as shown in Figure 5.11. This is a satisfying result, since the model was not calibrated and we used a simplified approach, where the K_s of the aquifer was assumed to be isotropic and homogeneous.

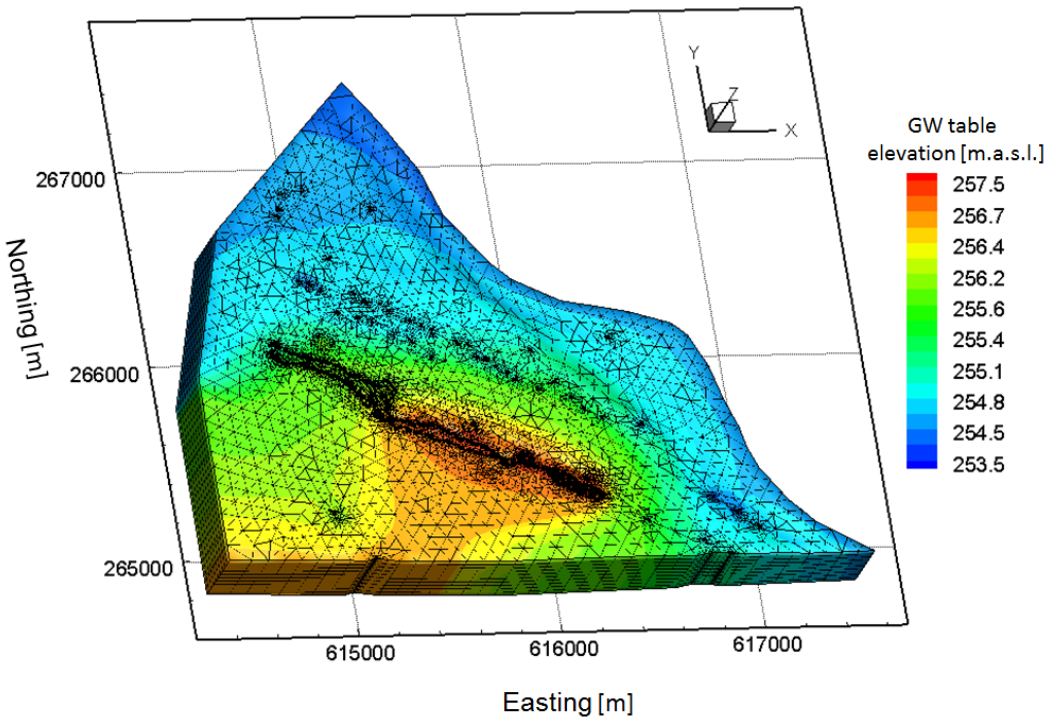

Figure 5.10: Simulated groundwater table elevations in the study area.

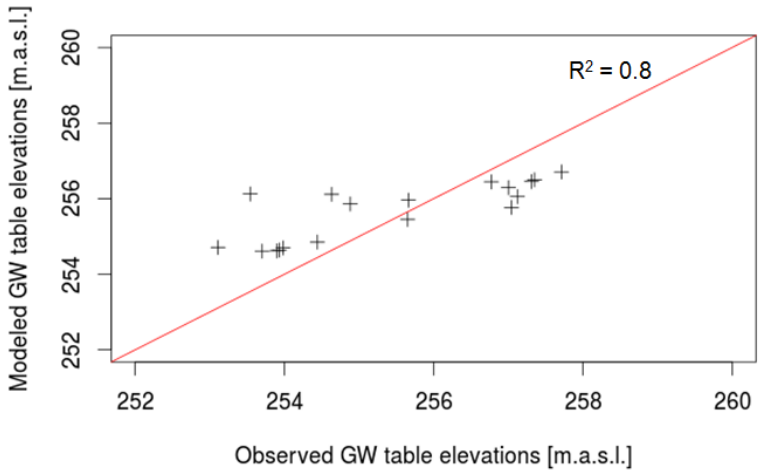

Figure 5.11: Simulated versus observed groundwater table elevations.

Table 5.4: The settings and effects on the groundwater table elevations around the last segments of the three scenarios.

Scenario	Setting	Effect
1:	20% increased flux at channels 7 and 8, and ponds 4, 5 and 6	no
2:	200% increased flux at channels 7 and 8, and ponds 4, 5 and 6	yes
3:	Scenario 1 + half cut pumping at western wells	yes

We were able to simulate the groundwater table elevations, which are the highest around the channels of the infiltration system and further south. This proves the existence of the build-up of a groundwater mound. However, the elevations close to the last segments show no distinct difference to the elevations of the surrounding area. This indicates that the built groundwater mound close to the last segments might not be sufficient to prohibit potentially contaminated water flowing to the pumping wells. In fact, the highest concentrations of contaminants were found at the down gradient of the western pumping wells. Consequently, we used the 3D model to simulate different scenarios where either the pumping rates of the affected wells were reduced or the water levels at channels 7 and 8 were increased.

Altogether, we simulated three scenarios. Figures 5.12 and 5.13 illustrate the streamtraces and groundwater table elevations for the original conditions (a) as well as for scenarios 1 to 3 (b–d). The streamtraces visualize the water flow directions within the model domain.

The first scenario implies an increased specified flux of 20% at channels 7 and 8, and pond 4. We can see in Figure 5.12b that there are no relevant changes in the flow direction (shown by the stream traces) or the groundwater table elevations compared to Figure 5.12a, which represents the original groundwater table elevations.

To obtain a recognizable effect, we doubled the original infiltration rate in the second scenario. The results indicate that this scenario led to a slightly higher groundwater mound around channels 7 and 8, and in the southern part of the model domain, compared to the previous simulations.

In scenario 3, we simulated the conditions of scenario 1 in addition to decreased (-50%) pumping at the western water abstraction wells. With these combined measures the flow directions seem to stay the same, however the groundwater table elevations are higher compared to the original conditions and scenario 1. Table 5.4 gives a summarized overview of the settings of the three different scenarios and the

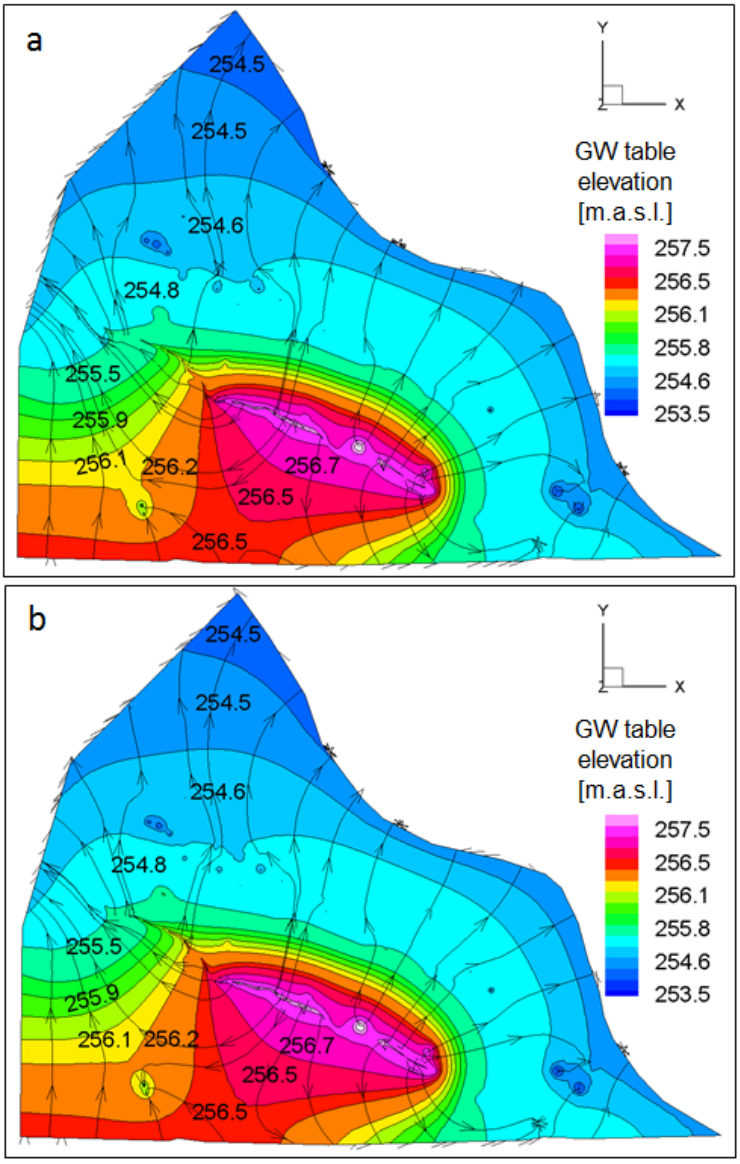

Figure 5.12: Groundwater table elevations for the original case (a) and scenario 1 (b: 20% increased flux at the last segments).

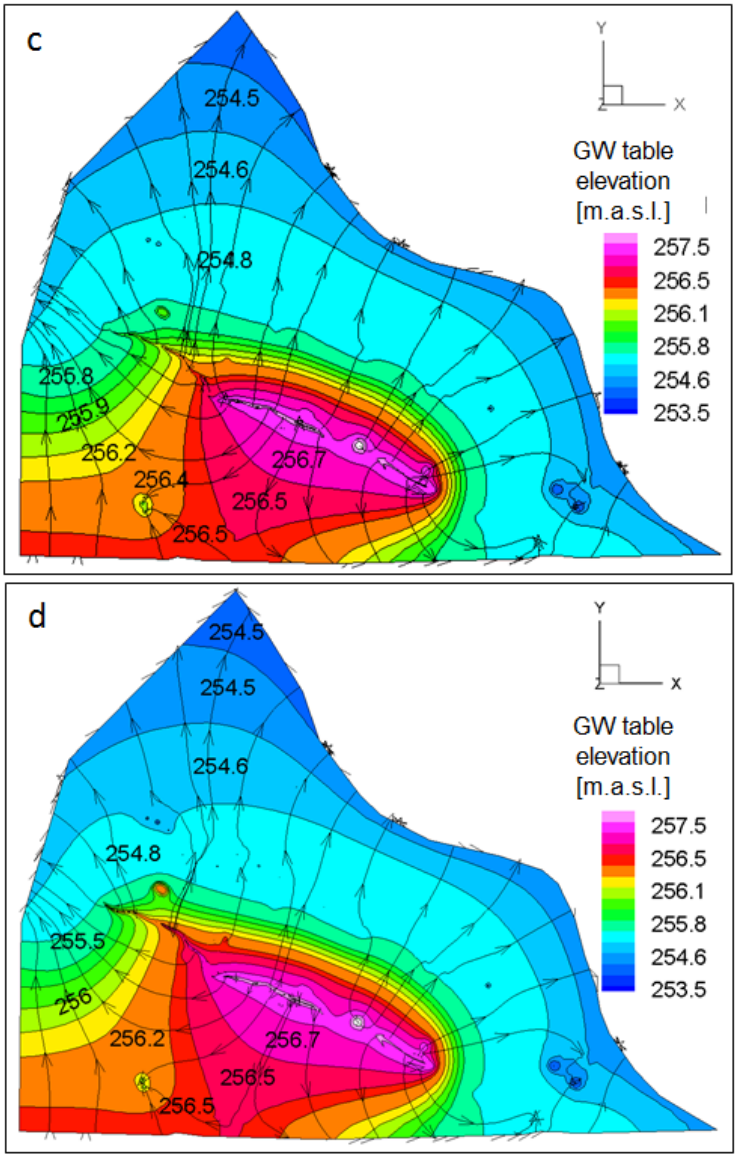

Figure 5.13: Groundwater table elevations for scenario 2 (c: 200% increased flux at the last segments) and scenario 3 (d: scenario 1 plus pumping cut by half at western wells).

obtained effects.

To investigate the effect of the increased groundwater table elevations on the contaminant concentration, transport modeling would be necessary. Additionally, the interpretation of the model results are limited in the way that the model does not consider the complex geologic structure with karstic structures at the presented study site. This is an important fact to consider when simulating transport processes. Hence, the transport of contaminants could not be investigated with this simplified model approach. However, transport modeling was not the purpose of this study.

6

Conclusions and Outlook

The objective of this study was to characterize the spatial and temporal artificial groundwater recharge at the Hardwald by a combination of field testing and numerical modeling. Several conclusions could be drawn, but further investigations would be necessary to confirm the findings of this study.

6.1 Conclusions

With this master's thesis we were able to explain the processes and influencing factors controlling groundwater recharge at Hardwald. In the following, the key findings of this study are summarized:

- Field testing showed that the spatial recharge is highly heterogeneous which mainly depends on the distribution of water levels at the infiltration system. The channels and ponds with the highest water levels correlate with those of the highest infiltration rates. Furthermore, the temporal infiltration rates for the analyzed time series are relatively stable despite occasional fluctuations of the water levels.

- The analysis conducted with the cross-section model revealed that the system is highly sensitive to the depth of the groundwater table, the clogging layer thickness and the saturated hydraulic conductivity of the clogging layer and aquifer material. The flux regime at the study site is disconnected.

- From the scenario modeling with the 3D model it can be concluded that the

groundwater table elevations only show a slight to no sensitivity to increased water levels in the last segments of the study area. An increased infiltration at the western segment of the infiltration system only has an effect on the groundwater table elevations in combination with reduced pumping rates.

6.2 Outlook

Additional investigations regarding the clogging layer material and thickness should be conducted, since the properties of the confined streambed are important factors for the infiltration rate. Field testings or the analysis of existing drilling cores might give more precise information about the properties of these parameters.

Furthermore, transport modeling is necessary to investigate the effect of increased water levels and different water abstraction rates on the concentrations of contaminants at the western part of the water abstraction wells.

The results of this thesis will be implemented in the groundwater management tool developed within sub-project 3 of the project "Regionale Wasserversorgung Basel-Landschaft 21".

Bibliography

Affolter, A., Zechner, E., and Huggenberger, P. (2010). Grundwassermodell Unteres Birstal - Rhein - Muttenz. https://www.baselland.ch/fileadmin/baselland/files/docs/bud/aue/grundwasser/form/grundwassermodell_bericht-bl_2010.pdf. January 26, 2015.

Auckenthaler, A., Bänninger, D., Affolter, A., Zechner, E., and Huggenberger, P. (2010). Drinking water production close to contaminant sites: a case study from the region of Basel, Switzerland. http://iahs.info/uploads/dms/abs_342_0167.pdf. January 05, 2015.

Bhuiyan, C. (2015). An approach towards site selection for water banking in unconfined aquifers through artificial recharge. *Journal of Hydrology*, 523:465–474.

Bouwer, H. (2002). Artificial recharge of groundwater: Hydrogeology and engineering. *Hydrogeology Journal*, 10(1):121–142.

Bruen, M. P. and Osman, Y. Z. (2004). Sensitivity of stream–aquifer seepage to spatial variability of the saturated hydraulic conductivity of the aquifer. *Journal of Hydrology*, 293(1-4):289–302.

Brunner, P., Cook, P. G., and Simmons, C. T. (2009a). Hydrogeologic controls on disconnection between surface water and groundwater. *Water Resources Research*, 45(1).

Brunner, P., Cook, P. G., and Simmons, C. T. (2011). Disconnected surface water and groundwater: From theory to practice. *Ground Water*, 49(4):460–467.

Brunner, P. and Simmons, C. T. (2012). HydroGeoSphere: A Fully Integrated, Physically Based Hydrological Model. *Ground Water*, 50(2):170–176.

Brunner, P., Simmons, C. T., and Cook, P. G. (2009b). Spatial and temporal aspects of the transition from connection to disconnection between rivers, lakes and groundwater. *Journal of Hydrology*, 376(1-2):159–169.

Calver, A. (2001). Riverbed permeabilities: information from pooled data. *Ground Water*, 39(4):546–553.

Cardenas, M. B. (2009). Stream-aquifer interactions and hyporheic exchange in gaining and losing sinuous streams. *Water Resources Research*, 45(6).

Carsel, R. and Parrish, R. (1988). Developing Joint Probability Distributions of Soil Water Retention Characteristics. *Water Resources Research*, 24(5):755–769.

Doble, R., Brunner, P., McCallum, J., and Cook, P. G. (2012). An analysis of river bank slope and unsaturated flow effects on bank storage. *Ground Water*, 50(1):77–86.

Doherty, J. (2010). PEST—Model-Independent Parameter Estimation (The PEST manual. http://www.pesthomepage.org/Downloads.php. March 25, 2015.

Fleckenstein, J. H., Niswonger, R. G., and Fogg, G. E. (2006). River-aquifer interactions, geologic heterogeneity, and low-flow management. *Ground Water*, 44(6):837–52.

Fox, G. A. and Durnford, D. S. (2003). Unsaturated hyporheic zone flow in stream/aquifer conjunctive systems. *Advances in Water Resources*, 26(9):989–1000.

Greskowiak, J., Prommer, H., Massmann, G., Johnston, C. D., Nützmann, G., and Pekdeger, A. (2005). The impact of variably saturated conditions on hydrogeochemical changes during artificial recharge of groundwater. *Applied Geochemistry*, 20(7):1409–1426.

Hatch, C. E., Fisher, A. T., Ruehl, C. R., and Stemler, G. (2010). Spatial and temporal variations in streambed hydraulic conductivity quantified with time-series thermal methods. *Journal of Hydrology*, 389(3-4):276–288.

Irvine, D. J., Brunner, P., Franssen, H.-J. H., and Simmons, C. T. (2012). Heterogeneous or homogeneous? Implications of simplifying heterogeneous streambeds in models of losing streams. *Journal of Hydrology*, 424-425:16–23.

Mair, A., Hagedorn, B., Tillery, S., El-Kadi, A. I., Westenbroek, S., Ha, K., and Koh, G. W. (2013). Temporal and spatial variability of groundwater recharge on Jeju Island, Korea. *Journal of Hydrology*, 501:213–226.

Matousek, Baumann, and Niggli AG (2011). Grundwasserbelastungen Hardwald (Muttenz) und Umgebung. https://www.baselland.ch/fileadmin/baselland/files/docs/bud/aue/grundwasser/form/mbn_grundwasserbelastung-hardwald_2010_bericht.pdf. December 16, 2014.

Mc Laren, R. G. (2011). GRID BUILDER A pre-processor for 2-D, triangular element, finite-element programs. Technical report, University of Waterloo.

Meier, T. (2014). Challenges of producing drinking water from infiltrated river water. http://www.eawag.ch/medien/publ/eanews/infotag_2014/tagungsband_e.pdf. December 12, 2014.

Morel-Seytoux, H. J., Mehl, S., and Morgado, K. (2014). Factors influencing the stream-aquifer flow exchange coefficient. *Ground Water*, 52(5):775–81.

Mualem, Y. (1976). A new model for predicting the hydraulic conductivity of unsaturated porous media. *Water Resources Research*, 12(3):513–522.

Osman, Y. Z. and Bruen, M. P. (2002). Modelling stream–aquifer seepage in an alluvial aquifer: an improved loosing-stream package for MODFLOW. *Journal of Hydrology*, 264:69–86.

OTT (2012). OTT MF pro Operating Instructions. http://www.ott.com/products/water-flow/ott-mf-pro/. March 2, 2015.

Pedretti, D., Barahona-Palomo, M., Bolster, D., Sanchez-Vila, X., and Fernàndez-Garcia, D. (2012). A quick and inexpensive method to quantify spatially variable infiltration capacity for artificial recharge ponds using photographic images. *Journal of Hydrology*, 430-431:118–126.

Petersen-Øverleir, A. (2005). A hydraulics perspective on the power-law stage-discharge rating curve. http://www.nve.no/Global/Publikasjoner/Publikasjoner2005/Report2005/report5-05.pdf. December 03, 2014.

Reitan, T. and Petersen-Øverleir, A. (2004). Estimating the discharge rating curve by nonlinear regression—The frequentist approach. http://www.nve.no/Global/Publikasjoner/Publikasjoner2004/Report2004/Trykkefilreport6-04.pdf. November 14, 2014.

Rivière, A., Gonçalvès, J., Jost, A., and Font, M. (2014). Experimental and numerical assessment of transient stream-aquifer exchange during disconnection. *Journal of Hydrology*, 517:574–583.

Sophocleous, M. (2002). Interactions between groundwater and surface water: The state of the science. *Hydrogeology Journal*, 10(1):52–67.

Stephens, D. (1976). *Vadose zone hydrology*. CRC Press, Florida, US.

Tecplot (2013). Tecplot 360 Getting Started Manual. http://www.scc.kit.edu/downloads/sca/tpgs.pdf. January 10, 2015.

Therrien, R., Mclaren, R. G., Sudicky, E. A., and Panday, S. M. (2010). HydroGeoSphere—A Three-dimensional Numerical Model Describing Fully-integrated Subsurface and Surface Flow and Solute Transport. *Draft*, 1.

Treese, S., Meixner, T., and Hogan, J. F. (2009). Clogging of an effluent dominated semiarid river: A conceptual model of stream-aquifer interactions. *Journal of the American Water Resources Association*, 45(4):1047–1062.

US Environmental Protection Agency (2012). Integrated Risk Information System (IRIS). http://www.epa.gov/ttnatw01/hlthef/tet-ethy.html. May 10, 2015.

van Genuchten, M. T. (1980). A Closed-form Equation for Predicting the Hydraulic Conductivity of Unsaturated Soils. *Soil Science Society of America Journal*, 44(5):892.

Winter, T. C. (1999). Relation of streams, lakes, and wetlands to groundwater flow systems. *Hydrogeology Journal*, 7(1):28–45.

WMO (2008). Guide to Hydrological Practices. http://www.whycos.org/hwrp/guide/. March 18, 2015.

Woessner, W. (2000). Stream and Fluvial Plain Ground Water Interactions: Rescaling Hydrogeologic Thought. *Ground Water*, 38(3):423–429.

A

Influence of Lateral Boundary Conditions

The distance of the lateral boundary conditions was investigated for a water level of 1 m, 0.5 m and 0.15 m (for all simulations a clogging layer thickness of 0.5 m was assumed). Figure A.1 shows that for the mean depth to the water table of 16 m at the study site and hence, a disconnected flow regime, there is no more influence of the later boundaries on the infiltration flux. Additionally, the infiltration curves for the different water levels show the influence on the infiltration rates.

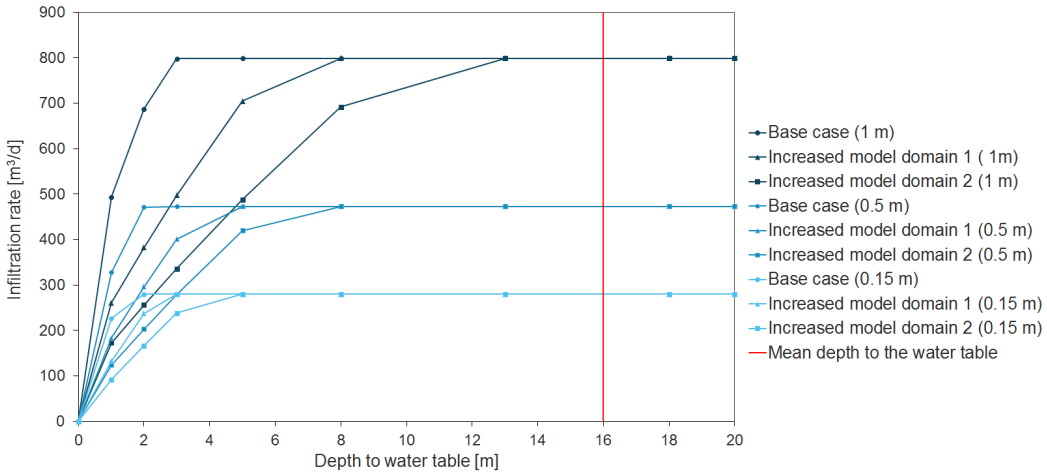

Figure A.1: Influence of increased model domain and different water levels on infiltration rates. Increased model domain 1: +300 m on every side; increased model domain 2: +500 m on every side. The red line represents the mean depth to the water table at the study site.

B

Example HydroGeoSphere Input Files

B.1 Cross-Section Model

The grok-file of the cross-section model (comments after "!"; two-column format):

Cross-section model (mean water levels)	73.625
end title	73.75
!2D (x, y) grid	73.875
Generate variable rectangles	74
96 ! number of nodes in x-direction	74.125
0 ! position of nodes in x	74.25
10	74.375
20	74.5
30	74.625
40	74.75
50	74.875
60	75
65	75.125
68	75.25
70	75.375
71	75.5
72	75.625
72.5	75.75
73	75.875
73.25	76
73.5	76.25

76.5
76.75
77
77.5
78
79
80
82
85
90
100
110
120
125
128
130
131
132
132.5
133
133.25
133.5
133.625
133.75
133.875
134
134.125
134.25
134.375
134.5
134.625
134.75
134.875
135
135.125
135.25
135.375
135.5
135.625
135.75
135.875
136
136.25
136.5
136.75
137
137.25
137.75
138.25
139.25
140.25
142.25
152.25
162.25
172.25
182.25
192.25
202.25
212.25
2 ! number of nodes in y-direction
0 ! position of nodes in y
549
!— Layers (set up for vertical discretisation)
GENERATE LAYERS INTERACTIVE
zone by layer
base elevation
elevation constant
0
end ! base elevation
new layer
layer name
layer 1

```
elevation constant
51 ! elevation of the top
Proportional sublayering
74 ! number of nodes in z-direction
!for HGS 51 !values for desired discretisation
divided by total thickness
0.000612745 ! 0.03125 50.96875 0.000612745
! 0.03125 50.9375
0.000612745 ! 0.03125 50.90625
0.000612745 ! 0.03125 50.875
0.000612745 ! 0.03125 50.84375
0.000612745 ! 0.03125 50.8125
0.000612745 ! 0.03125 50.78125
0.000612745 ! 0.03125 50.75
0.000612745 ! 0.03125 50.71875
0.000612745 ! 0.03125 50.6875
0.000612745 ! 0.03125 50.65625
0.000612745 ! 0.03125 50.625
0.000612745 ! 0.03125 50.59375
0.000612745 ! 0.03125 50.5625
0.000612745 ! 0.03125 50.53125
0.000612745 ! 0.03125 50.5
0.000612745 ! 0.03125 50.46875
0.000612745 ! 0.03125 50.4375
0.000612745 ! 0.03125 50.40625
0.000612745 ! 0.03125 50.375
0.000612745 ! 0.03125 50.34375
0.000612745 ! 0.03125 50.3125
0.000612745 ! 0.03125 50.28125
0.000612745 ! 0.03125 50.25
0.000612745 ! 0.03125 50.21875
0.000612745 ! 0.03125 50.1875
0.000612745 ! 0.03125 50.15625
0.000612745 ! 0.03125 50.125
0.000612745 ! 0.03125 50.09375
0.000612745 ! 0.03125 50.0625
0.000612745 ! 0.03125 50.03125
0.000612745 ! 0.03125 50
0.001960784 ! 0.1 49.9
0.001960784 ! 0.1 49.8
0.001960784 ! 0.1 49.7
0.001960784 ! 0.1 49.6
0.001960784 ! 0.1 49.5
0.004901961 ! 0.25 49.25
0.004901961 ! 0.25 49
0.004901961 ! 0.25 48.75
0.004901961 ! 0.25 48.5
0.004901961 ! 0.25 48.25
0.004901961 ! 0.25 48
0.009803922 ! 0.5 47.5
0.009803922 ! 0.5 47
0.009803922 ! 0.5 46.5
0.009803922 ! 0.5 46
0.009803922 ! 0.5 45.5
0.009803922 ! 0.5 45
0.009803922 ! 0.5 44.5
0.009803922 ! 0.5 44
0.009803922 ! 0.5 43.5
0.009803922 ! 0.5 43
0.009803922 ! 0.5 42.5
0.009803922 ! 0.5 42
0.009803922 ! 0.5 41.5
0.009803922 ! 0.5 41
0.009803922 ! 0.5 40.5
0.009803922 ! 0.5 40
0.019607843 ! 1 39
0.019607843 ! 1 38
0.019607843 ! 1 37
0.019607843 ! 1 36
0.019607843 ! 1 35
0.039215686 ! 2 33
0.039215686 ! 2 31
```

```
0.039215686 ! 2 29
0.039215686 ! 2 27
0.039215686 ! 2 25
0.098039216 ! 5 20
0.098039216 ! 5 15
0.098039216 ! 5 10
0.098039216 ! 5 5
0.098039216 ! 5 -7.10543E-15
end ! new layer
end ! generate layer interactive
end grid generation
Mesh to tecplot
mesh.dat
!— Boundary conditions
!— Right lateral boundary (constant head at boundary)
clear chosen nodes
choose nodes block
212.25 212.25 ! x
0 549 ! y
0 31 ! z
specified head
1
0 35.4 ! here specified head of well no. 21.C.223
!— left boundary (constant head at boundary)
clear chosen nodes
choose nodes block
0 0
0 549
0 31
specified head
1
0 34.3 ! here specified head of well no. 21.C.219
!— River (constant head boundary in channel 6 (ESD), 53cm)
clear chosen nodes
choose nodes block
74 76
0 549
50 51
specified head
1
0 50.53
!— River (constant head in channel 5 (ESD), 43cm)
!echo flow boundary conditions
clear chosen nodes
choose nodes block
134 136
0 549
49.5 51
specified head
1
0 49.93
!— Porous media properties
use domain type
porous media
properties file
material.mprops !name of the file storing material properties
!— Aquifer
clear chosen zones
choose elements all
new zone
1
choose zone number
1
read properties
Sand
```

```
!— Clogging layer for channel 5
clear chosen zones
clear chosen elements
choose elements block
73.5 76.5 !x
0 549 !y
49.5 50 !z
new zone
2
choose zone number
2
read properties
CloggingLayer
!— Clogging layer for channel 6
clear chosen zones
clear chosen elements
choose elements block
133.5 136.5
0 549
49 49.5
new zone
3
choose zone number
3
read properties
CloggingLayer
!— General simulation parameters
finite difference mode
unsaturated
units: kilogram-metre-day
!transient flow
!dual nodes for surface flow
!— Newton iteration parameters compute
underrelaxation factor
Newton maximum iterations
10000
Jacobian epsilon
0.000001
Newton absolute convergence criteria
1.0d-4
Newton residual convergence criteria
1.0d-4
Newton maximum update for head
0.05
Flow solver maximum iterations
1000
!— Output
output times
1
end
```

B.2 3D Model

The grok-file of the 3D model:

```
Hardwald end title !Grid generation read
gb 2d grid !reads 2D grid established with
GRIDBUILDER
./grid/grid_2015-03-21
generate layers interactive ! 3D grid genera-
tion
zone by layer
Base elevation
elevation constant
150 !Min Sohle KOT at 178masl
End
new layer
```

```
layer name
Top layer
uniform sublayering
10
Elevation from gb file !reads digital elevation
model ./topo/grid_2015-03-21.nprop.topo
end
end ! generate layers interactive
end grid generation
!— General simulation parameters
units: kilogram-metre-day
!transient flow
!— Porous media properties
use domain type
porous media
properties file
aquifer_CL.mprops
!— Aquifer
clear chosen zones
choose elements all
new zone
1
choose zone number
1
read properties
Sand
!— Boundary conditions assigned in GRID-
BUILDER
! Lower BC
clear chosen nodes
choose nodes gb
./BC/grid_nchos.LowerBC_left
1 7
Function x head
614365 256.5
615406 256.5
clear chosen nodes
choose nodes gb
./BC/grid_nchos.LowerBC_right
1 7
Function x head
615406 256.5
617545 254.52
! Rhein BC
clear chosen nodes
choose nodes gb
./BC/grid_nchos.RheinBC
1 7
Function x head
617545 254.52
615351 254.46
! West BC
clear chosen nodes
choose nodes gb
./BC/grid_nchos.WestBC_J89-C241
1 7
Function x head
614365 256.5
614384 254.6
clear chosen nodes
choose nodes gb
./BC/grid_nchos.WestBC_C241-Rhein
1 7
Function x head
614384 254.6
615351 254.46
!— Channels/pond (l/day) !Channel 1 (ESA)
clear chosen faces
Choose faces top gb
./BC/grid_echos.ESA_2015-03-22
specified flux
1
```

```
0 12.9
!Channel 2 (1EZ)
clear chosen faces
Choose faces top gb
./BC/grid_echos.1EZ_2015-03-22
specified flux
1
0 15.6
!Channel 3 (ESB)
clear chosen faces
Choose faces top gb
./BC/grid_echos.ESB_2015-03-22
specified flux
1
0 13.3
!Pond1
clear chosen faces
Choose faces top gb
./BC/grid_echos.Pond1_2015-03-22
specified flux
1
0 1.7
! Channel 4 (2EZ)
clear chosen faces
Choose faces top gb
./BC/grid_echos.InterStream1_2015-03-23
specified flux
1
0 6.9
!Pond 2 (6)
clear chosen faces
Choose faces top gb
./BC/grid_echos.Pond6_2015-03-23
specified flux
1
0 4.2
! Channel 5 (ESC-ASC)
clear chosen faces
Choose faces top gb
./BC/grid_echos.ESC_2015-03-23
specified flux
1
0 29.70
!Pond 3 (5)
clear chosen faces
Choose faces top gb
./BC/grid_echos.Pond5_2015-03-23
specified flux
1
0 0.62
! Channel 6 (ESD–ASD)
clear chosen faces
Choose faces top gb
./BC/grid_echos.ESD_2015-03-23
specified flux
1
0 1.70
!Channel 7 (ESE–end)
clear chosen faces
Choose faces top gb
./BC/grid_echos.ESE_2015-03-23
specified flux
1
0 0.39
!Pond 4 (3)
clear chosen faces
Choose faces top gb
./BC/grid_echos.Pond3_2015-03-23
specified flux
1
0 0.55
!Pond4
```

clear chosen faces
Choose faces top gb
./BC/grid_echos.Pond4_2015-03-23
specified flux
1
0 0.56
!Channel 8 (ESF–end)
clear chosen faces
Choose faces top gb
./BC/grid_echos.ESF_2015-03-23
specified flux
1
0 6.40
!Pond 5 (7)
clear chosen faces
Choose faces top gb
./BC/grid_echos.Pond7_2015-03-23
specified flux
1
0 0.26
!— Obeservation points (gw head output)
Make observation point
21.C.215
615500 265667 244.33
Make observation point
21.C.222
615173 265527 254.11
Make observation point
21.C.223
615500 265440 247.28
Make observation point
21.C.228
615833 265138 248.7
Make observation point
21.C.234
615681 265735 243.4
Make observation point
21.C.43
615925 265692 240.88
Make observation point
21.C.235
616170 265451 242.88
Make observation point
21.C.240
614514 266180 247.65
Make observation point
21.C.80
614860 265590 247.5
Make observation point
21.C.18
615364 266584 227.5
Make observation point
21.J.89
614365 264925 209.12
Make observation point
21.C.210
615540 265906 241.54
Make observation point
21.C.229
616207 265050 250
Make observation point
21.C.206
614700 266215 243.2
Make observation point
21.C.16
615639 266422 241.12
Make observation point
21.C.219
615250 265850 253.66
Make observation point
21.C.36
615208 266660 238.54

Make observation point
21.C.71
614969 266481 229.44
!— Pumping wells with mean pumping rates
Make well
21.A.1
615266 266137 269.8
615266 266137 232.9
1
0 -2735
615266 266137 252.9
0.4
0.4
Make well
21.A.4
614947 266357 271.35
614947 266357 231.65
1
0 -1859
614947 266357 231.65
0.4
0.4
Make well
21.A.5
614995 266339 270.4
614995 266339 241.3
1
0 -1962
614995 266339 241.3
0.4
0.4
Make well
21.A.6
615044 266303 271.33
615044 266303 240.13
1
0 -1910
615044 266303 240.13
0.4
0.4
Make well
21.A.7
615114 266466 270
615114 266466 243.89
1
0 -299
615114 266466 243.89
0.4
0.4
Make well
21.A.9
615201 266285 272.36
615201 266285 239.16
1
0 -312
615201 266285 239.16
0.4
0.4
Make well
21.A.10
615251 266236 273
615251 266236 231.7
1
0 -277
615251 266236 231.7
0.4
0.4
Make well
21.A.11
615321 266231 272.1
615321 266231 233.1
1

0 -391
615321 266231 233.1
0.4
0.4
Make well
21.A.12
615357 266192 272.08
615357 266192 233.2
1
0 -1153
615357 266192 233.2
0.4
0.4
Make well
21.A.13
615407 266156 273
615407 266156 234.49
1
0 -287
615407 266156 234.49
0.4
0.4
Make well
21.A.14
615456 266139 272.08
615456 266139 233.5
1
0 -2351
615456 266139 233.5
0.4
0.4
Make well
21.A.15
615510 266115 271.9
615510 266115 237.81
1
0 -322
615510 266115 237.81
0.4
0.4
Make well
21.A.16
615551 266088 272.04
615551 266088 231.1
1
0 -1338
615551 266088 231.1
0.4
0.4
Make well
21.A.17
615665 266022 272.5
615665 266022 231.25
1
0 -283
615665 266022 231.25
0.4
0.4
Make well
21.A.18
615725 266009 272.81
615725 266009 234.6
1
0 -344
615725 266009 234.6
0.4
0.4
Make well
21.A.19
615752 265951 272.94
615752 265951 232.75
1

0 -2090
615752 265951 232.75
0.4
0.4
Make well
21.A.20
615793 265930 274.45
615793 265930 234.41
1
0 -1500
615793 265930 234.41
0.4
0.4
Make well
21.A.21
615835 265894 274.2
615835 265894 237.1
1
0 -1716
615835 265894 237.1
0.4
0.4
Make well
21.A.22
615880 265860 273.93
615880 265860 239.72
1
0 -1411
615880 265860 239.72
0.4
0.4
Make well
21.A.23
615926 265829 274.13
615926 265829 238.9
1
0 -2017
615926 265829 238.9
0.4
0.4
Make well
21.A.24
616022 265777 274.83
616022 265777 233.37
1
0 -261
616022 265777 233.37
0.4
0.4
Make well
21.A.26
616116 265815 274.1
616116 265815 236.4
1
0 -266
616116 265815 236.4
0.4
0.4
Make well
21.A.27
616180 265732 274.7
616180 265732 234.25
1
0 -345
616180 265732 234.25
0.4
0.4
Make well
21.A.28
616226 265673 274.8
616226 265673 238.5
1

0 -1386
616226 265673 238.5
0.4
0.4
Make well
21.A.29
616314 265628 274.8
616314 265628 237.54
1
0 -1026
616314 265628 237.54
0.4
0.4
Make well
21.A.30
615363 266069 271.01
615363 266069 232.21
1
0 -1443
615363 266069 232.21
0.4
0.4
Make well
21.A.31
615440 266040 270
615440 266040 235.6
1
0 -1506
615440 266040 235.6
0.4
0.4
Make well
21.A.32
615528 265953 269.53
615528 265953 240.83
1
0 -1493
615528 265953 240.83
0.4
0.4
Make well
21.A.33
615110 266190 272.45
615110 266190 232.24
1
0 -1910
615110 266190 232.24
0.4
0.4
Make well
21.A.34
615200 266165 270.82
615200 266165 225.32
1
0 -502
615200 266165 225.32
0.4
0.4
Make well
21.A.104
616501 265591 267.25
616501 265591 235.7
1
0 -4391
616501 265591 235.7
0.4
0.4
Make well
21.A.105
616448 265095 275
616448 265095 206.7
1

0 -2714
616448 265095 206.7
0.4
0.4
Make well
21.E.20
616899 265144 260.3
616899 265144 240.2
1
0 -3650
616899 265144 240.2
0.4
0.4
Make well
21.E.23
616801 265224 262.1
616801 265224 203.1
1
0 -7120
616801 265224 203.1
0.4
0.4
Make well
21.E.24
616999 265067 253.5
616999 265067 199.31
1
0 -0
616999 265067 199.31
0.4
0.4
Make well
21.E.27
616737 264925 268.83
616737 264925 178.03
1
0 -30
616737 264925 178.03
0.4
0.4
Make well
21.E.28
616717 264986 268.82
616717 264986 179.32
1
0 -4850
616717 264986 179.32
0.4
0.4
Make well
21.E.21
616833 264922 267.97
616833 264922 199.27
1
0 -4440
616833 264922 199.27
0.4
0.4
Make well
21.E.3
614935 265124 278.27
614935 265124 231.27
1
0 -2229
614935 265124 231.27
0.4
0.4
Make well
21.E.4
614926 265161 278.21
614926 265161 225.01
1

0 -2680
614926 265161 225.01
0.4
0.4
Make well
17.E.11
615047 266832 252.95
615047 266832 243.3
1
0 -86.4
615047 266832 243.3
0.4
0.4
!— Newton iteration parameters
compute underrelaxation factor
Newton maximum iterations
10000
Jacobian epsilon
0.000001
Newton absolute convergence criteria
1.0d-4
Newton residual convergence criteria
1.0d-4
Newton maximum update for head
0.05
Flow solver maximum iterations
1000
!— Output
output times
1
end

Declaration on Scientific Integrity
Erklärung zur wissenschaftlichen Redlichkeit

I hereby declare that I wrote this thesis on my own, only making use of the sources mentioned and marking all parts taken from published works. Additionally, I confirm that this thesis has not been prepared for a different exam, neither in parts nor in its entirety.

Hiermit erkläre ich, dass ich diese Abschlussarbeit selbstständig verfasst habe, keine anderen als die angegebenen Quellen/Hilfsmittel verwendet habe und alle Stellen, die wörtlich oder sinngemäß aus veröffentlichten Schriften entnommen wurden, als solche kenntlich gemacht habe. Darüber hinaus erkläre ich, dass diese Abschlussarbeit nicht, auch nicht auszugsweise, bereits für eine andere Prüfung angefertigt wurde.

Freiburg, Juni 2015

Signature — Unterschrift